HHS Public Access

Author manuscript

Nat Metab. Author manuscript; available in PMC 2019 August 13.

Published in final edited form as:

Nat Metab. 2019 January ; 1(1): 98–110. doi:10.1038/s42255-018-0004-9.

The long noncoding RNA CHROME regulates cholesterol homeostasis in primate

Elizabeth J. Hennessy[#1], **Coen van Solingen**[#1], **Kaitlyn R. Scacalossi**[1], **Mireille Ouimet**[1], **Milessa S. Afonso**[1], **Jurrien Prins**[2], **Graeme J. Koelwyn**[1], **Monika Sharma**[1], **Bhama Ramkhelawon**[1], **Susan Carpenter**[3], **Albert Busch**[4,5], **Ekaterina Chernogubova**[4], **Ljubica Perisic Matic**[4], **Ulf Hedin**[4], **Lars Maegdefessel**[4,5], **Brian E. Caffrey**[6], **Maryem A. Hussein**[7], **Emiliano P. Ricci**[8], **Ryan E. Temel**[9], **Michael J. Garabedian**[7], **Jeffrey S. Berger**[1], **Kasey C. Vickers**[10], **Matthew Kanke**[11], **Praveen Sethupathy**[11], **Daniel Teupser**[12], **Lesca M. Holdt**[12], **Kathryn J. Moore**[1]

[1]Department of Medicine, Leon H. Charney Division of Cardiology, New York University School of Medicine, New York, New York, USA. [2]Department of Internal Medicine (Nephrology), Einthoven Laboratory for Vascular and Regenerative Medicine, Leiden University Medical Center, Leiden, The Netherlands. [3]Department of Molecular, Cell and Developmental Biology, University of California, Santa Cruz, California, USA. [4]Department of Molecular Medicine and Surgery, Karolinska Institute, Stockholm, Sweden. [5]Department of Vascular and Endovascular Surgery, Klinikum Rechts der Isar, Technical University Munich, Munich, Germany. [6]Max Planck Institute for Molecular Genetics, Berlin, Germany. [7]Department of Microbiology, New York University School of Medicine, New York, New York, USA. [8]INSERM U1111, Centre International de Recherche en Infectiologie, Ecole Normale Supérieure de Lyon, Université de Lyon, Lyon, France. [9]Saha Cardiovascular Research Center, University of Kentucky, Lexington, Kentucky, USA. [10]Department of Medicine, Vanderbilt University Medical Center, Nashville, Tenessee, USA. [11]Department of Biomedical Sciences, College of Veterinary Medicine, Cornell University Ithaca, New York, USA. [12]Institute of Laboratory Medicine, Ludwig-Maximilians-University Munich, Munich, Germany.

[#] These authors contributed equally to this work.

Corresponding Author: Correspondence and requests for materials should be addressed to: Kathryn J. Moore, PhD, New York University Langone Health, 435 E 30th Street, Science Building 706, New York, NY 10016, USA. kathryn.moore@nyumc.org.

Author Contributions: E.J.H., C.vS. and K.J.M. designed the study, guided the interpretation of the results and prepared the manuscript, with input from all authors. E.J.H. and C.vS. performed experiments and data analyses. K.R.S., M.O., M.S.A., J.P., G.J.K., M.S., B.R., K.C.V., M.K. and P.S. contributed to experiments and data analyses. S.C. created and analyzed stable cell lines. A.B. and M.O. performed *in situ* hybridization of human plaques. E.C., L.P.M., U.H. and L.M. processed and analyzed BiKE datasets. B.E.C. performed RNAcofold and RNAhybrid analyses. E.P.R. performed polysome fractionation experiments. R.E.T. supervised non-human primate studies. M.A.H. and M.J.G. performed ChIP experiments. J.S.B. provided human plasma samples and assisted in data interpretation. D.T. and L.M.H. performed human liver RNA and lipoprotein analyses.

Data Availabilty

The Biobank of Karolinska Endarterectomies (BiKE) microarray dataset is deposited in the Gene Expression Omnibus (GEO) and available under accession GSE21545. HepG2 RNA-sequencing datasets are deposited in GEO under accession GSE97469. Data that supports the plots within this paper and other findings of this study are available from the corresponding author upon reasonable request.

Competing Interests: KJM and New York University hold a patent (US 9241950, Status: issued 1/26/2016) on the use of miR-33 inhibitors to treat inflammation. All other authors have no competing interests.

Abstract

The human genome encodes thousands of long non-coding RNAs (lncRNAs), the majority of which are poorly conserved and uncharacterized. Here we identify a primate-specific lncRNA (*CHROME*), elevated in the plasma and atherosclerotic plaques of individuals with coronary artery disease, that regulates cellular and systemic cholesterol homeostasis. LncRNA *CHROME* expression is influenced by dietary and cellular cholesterol via the sterol-activated liver X receptor transcription factors, which control genes mediating responses to cholesterol overload. Using gain- and loss-of-function approaches, we show that *CHROME* promotes cholesterol efflux and HDL biogenesis by curbing the actions of a set of functionally related microRNAs that repress genes in those pathways. *CHROME* knockdown in human hepatocytes and macrophages increases levels of miR-27b, miR-33a, miR-33b and miR-128, thereby reducing expression of their overlapping target gene networks and associated biologic functions. In particular, cells lacking *CHROME* show reduced expression of ABCA1, which regulates cholesterol efflux and nascent HDL particle formation. Collectively, our findings identify *CHROME* as a central component of the non-coding RNA circuitry controlling cholesterol homeostasis in humans.

The maintenance of cholesterol homeostasis is essential to human health, and its dysregulation results in disease states, including atherosclerotic cardiovascular disease[1]. The removal of excess cholesterol from cells and its delivery to the liver via high density lipoproteins (HDL) are central in protecting from pathologic cholesterol deposition in tissues, particularly the artery wall where atherosclerotic plaques form[2]. Understanding the regulatory circuits that contribute to the dynamic and temporal balancing of cholesterol at the cellular and organismal level are thus of critical importance. At the transcriptional level, the sterol-activated liver-X-receptors (LXR) have been shown to play key roles in the regulation of genes that control the response to cholesterol excess, particularly the cholesterol transporter ABCA1, which mediates cholesterol efflux and HDL biogenesis[3]. In addition, recent studies indicate that multiple classes of non-coding RNAs, including microRNAs (miRNAs), small nucleolar RNAs, and long non-coding RNAs (lncRNAs) possess regulatory functions that feed into the previously described networks controlling cellular lipid metabolism[4–6].

Among the non-coding RNAs, miRNAs have emerged as potent regulators of cholesterol homeostasis through their ability to repress the expression of genes in the integrated pathways of cholesterol and fatty acid biosynthesis, reverse cholesterol transport, and lipid storage[6]. One of the first such miRNAs to be identified was miR-33 (mmu-miR-33–5p; hsa-miR-33a-5p and hsa-miR-33b-5p), which was shown to reduce cholesterol efflux and reverse cholesterol transport by targeting genes involved in cholesterol export (e.g., *ABCA1*)[7,8], intracellular trafficking (e.g., *NPC1, OSBPL6, ATG5*)[8,9], and bile secretion (e.g., *ATP8B1, ABCB11*)[10]. The identification of miR-27b and miR-144 as additional repressors of genes regulating cholesterol efflux (e.g., *ABCA1, OSBPL6*)[9,11–14], and the demonstration that delivery of modified oligonucleotide inhibitors of miR-33 and miR-144 in mice could increase plasma levels of HDL cholesterol, underscored the importance of miRNAs as post-transcriptional regulators of cellular and systemic cholesterol homeostasis. Indeed, the relevance of this mechanism in regulating cholesterol metabolism in humans is supported by genome-wide association studies that have uncovered variants in miRNA loci

associated with abnormal lipoprotein levels and cardiometabolic disease risk[15]. One such example is miR-128, which was found to target *ABCA1* and *LDLR*, and consequently, to regulate plasma levels of HDL and low density lipoprotein (LDL) cholesterol, respectively[15]. However, given the redundancy in miRNA targeting of cholesterol efflux pathways described above, it remains unclear if such functionally related miRNAs are coordinately controlled or regulated by higher order systems.

LncRNAs contribute to regulatory complexity in higher eukaryotes through diverse mechanisms, including by regulating chromosomal architecture, facilitating the formation of ribonucleoprotein complexes, altering the epigenetic landscape of the genome, and mediating transcriptional and post-transcriptional gene regulation[16]. LncRNAs are broadly defined as non-protein coding RNA transcripts of greater than 200 nucleotides, and they can execute their functions by forming lncRNA-DNA, lncRNA-protein and lncRNA-RNA interactions in the nucleus and/or cytoplasm. While it is estimated that the human genome contains >10,000 lncRNAs, fewer than 5% of human lncRNAs have been functionally characterized, in part, because poor conservation among species has hindered their investigation[17,18]. Functional roles for lncRNAs in regulating cholesterol metabolism and cardiovascular disease are beginning to emerge[5,19]. For example, several lncRNAs have been identified that promote or inhibit the function of the sterol response element binding protein (SREBP) transcription factors that regulate genes involved in cholesterol and fatty acid synthesis, including MALAT1[20], H19[21], lncHR1[22], and *LeXis*[23]. Other lncRNAs, such as *MeXis*[24], have been shown to confer cell type selective expression of genes (e.g., *ABCA1*) by regulating the chromosomal architecture. Notably, the majority of cardiovascular disease-associated sequence variants identified from human genome wide association studies are found in the non-coding landscape of the genome, as is the case for the locus on chromosome 9p21 containing lncRNA ANRIL[25,26], which has the highest association with atherosclerotic risk and cardiovascular events. Understanding the functional significance of non-coding RNAs contributing to disease remains a major challenge.

Here we describe a primate-specific lncRNA, increased in the setting of human atherosclerotic vascular disease, that contributes to the maintenance of cholesterol homeostasis. Studies in non-human primates show that expression of lncRNA *CHROME* is upregulated in response to a cholesterol-enriched diet and by activation of the LXR transcription factor that coordinates the response to cholesterol excess. Using loss- and gain-of-function, we establish that *CHROME* increases the efflux of excess cholesterol from cells and promotes hepatic HDL biogenesis by curbing the actions of a set of miRNAs, which share the ability to repress genes involved in cholesterol efflux and reverse cholesterol transport. Consistent with these mechanistic studies, we find that hepatic levels of *CHROME* are inversely correlated with those of its miRNA targets, and positively correlated with plasma levels of HDL-C in a human cohort. In summary, our identification of *CHROME* unveils the regulatory cross-talk between non-coding RNAs that sustains cholesterol homeostasis in humans in health and disease.

Results

CHROME is a primate-specific lncRNA increased in atherosclerotic vascular disease

LncRNA AC009948.5 (ENSG00000223960), which we have named *CHROME* (**C**holesterol **H**omeostasis **R**egulator **o**f **M**iRNA **E**xpression), is proximal to a locus on human chromosome 2 linked to premature coronary artery disease[27] and plasma HDL-C levels[28]. The *CHROME* locus contains primate-specific *Alu* transposable repeat elements[29], and *CHROME* exons are conserved in primates, but are largely absent in other placental mammals or vertebrates (Fig. 1a, Supplementary Fig. 1a-c). We identified 7 splice variants of *CHROME* (Fig. 1a), which were broadly expressed in human tissues and cell types (Supplementary Fig. 2a-c). To test whether *CHROME* expression is altered in the setting of atherosclerotic vascular disease, we measured its expression in the plasma and arteries of individuals with coronary artery disease and healthy control subjects. Plasma levels of *CHROME,* measured by quantitative PCR (qPCR) using primers directed to a common region in all variants, were found to be markedly elevated in individuals with coronary artery disease compared to healthy individuals (Fig. 1b), whereas *LIPCAR* and *TapSAKI* (other known circulating lncRNAs) were unchanged (Supplementary Fig. 3a). Furthermore, analysis of *CHROME* expression in the Biobank of Karolinska Endarterectomies (BiKE) Affymetrix microarray datasets[30] showed that *CHROME* RNA levels were increased in atherosclerotic plaques from patients with symptomatic and asymptomatic carotid stenosis compared to control arterial samples (Fig. 1c). This was confirmed by qPCR for individual *CHROME* variants using exon-spanning primers complementary to unique sequences present in each of the *CHROME* isoforms (Supplementary Fig. 3b). To understand the cellular distribution of *CHROME* in the healthy and diseased artery wall, we performed RNA *in situ* hybridization. We found that in carotid artery plaques *CHROME* RNA (shown in blue) was localized to infiltrating inflammatory cells in both the neointima and areas of plaque rupture (Fig. 1d, boxed regions, Supplementary Fig. 3c). By contrast, there was little detectable *CHROME* RNA in the normal artery wall (Fig. 1e, Supplementary Fig. 3d). Together, these data suggest a potential function for *CHROME* in the setting of atherosclerotic vascular disease.

CHROME is upregulated in response to excess dietary or cellular cholesterol via LXR

To test whether *CHROME* expression is responsive to dietary and cellular cholesterol levels, we measured its expression in the livers of non-human primates prior to and after feeding of a diet enriched in cholesterol for 8 weeks. We observed that increasing dietary cholesterol levels increased the expression of *CHROME-1, CHROME-3* and *CHROME-7* in the liver - a tissue central to the regulation of systemic cholesterol homeostasis - compared to low fat chow diet feeding (Fig. 2a). We found that *CHROME* was abundantly expressed in primary human hepatocytes (10^2 copies/cell; Supplementary Fig 4a) and levels of *CHROME* variants increased with cyclodextrin-cholesterol treatment, compared to vehicle treatment (Fig. 2b). In addition to hepatocytes, macrophages play key roles in cholesterol homeostasis, particularly in the atherosclerotic plaque where they are recruited to clear accumulated LDL[31]. In human THP-1 monocytic cells differentiated into macrophages *in vitro*, *CHROME* is present at more than 10^2 copies/cell (Supplementary Fig. 4a), and its expression levels increased upon cholesterol loading with acetylated LDL (Fig. 2c). Using

prediction algorithms to uncover potential transcriptional regulators of *CHROME*, we identified putative binding sites for the sterol-activated LXR transcription factors (Supplementary Fig. 4b), which coordinate the expression of genes involved in cellular and systemic responses to cholesterol excess[3]. We performed chromatin immunoprecipitation in THP-1 macrophages treated with LXR agonist and observed LXR occupancy at the *CHROME* locus, at sites upstream of the start site of transcription and within the first intron (Fig. 2d). The levels of LXR enrichment over IgG control at these two sites in the *CHROME* locus were similar in magnitude to that found for the known LXR-responsive gene *OSBPL6*, which served as a positive control (Fig. 2d). Consistent with a role for LXR in regulating *CHROME* transcription, treatment of non-human primates with the LXR agonist GW3965 increased levels of *CHROME-1, CHROME-3, CHROME-4* and *CHROME-7* in the liver, as compared to control vehicle treatment (Fig. 2e). Furthermore, treatment of primary human hepatocytes, HepG2 cells and THP-1 macrophages with the LXR agonist T0901317 increased expression of *CHROME* variants compared to vehicle treatment (Fig. 2f, Supplementary Fig. 4c). Notably, treatment with T0901317 or acetylated LDL failed to increase *CHROME* or the control gene *ABCA1* in THP-1 macrophages when LXRα/β were silenced using siRNAs (Fig. 2g, Supplementary Fig. 4d). Together, these data identify *CHROME* as part of the network of genes regulated by LXR in primates in the settings of excess dietary or cellular cholesterol.

CHROME knockdown in hepatocytes reveals roles in cholesterol metabolism

To determine *CHROME*'s function, we first examined its subcellular distribution pattern as this can provide insight into the potential biological role of a lncRNA[32]. Using fluorescence *in situ* hybridization (FISH), we found that *CHROME* transcripts were distributed both in the nucleus and the cytoplasm in HEK293T cells (Fig. 3a), THP-1 macrophages (Supplementary Fig. 4e) and HepG2 cells (not shown). *CHROME*'s localization to the cytoplasm, the site of RNA translation, raised the possibility that it may contain an actively translated open reading frame. However, coding potential and Kozak sequence prediction algorithms indicated low coding potential of *CHROME* (Supplementary Fig. 5a-b, Supplementary Table 1), and this was confirmed by polysome fractionation in THP-1 macrophages (Supplementary Fig. 5c, d). To test the effect of *CHROME* loss-of-function, we used shRNAs, which preferentially deplete cytoplasmic lncRNAs[33], targeting a region of exon 1 common to all *CHROME* variants (Supplementary Fig. 6a). Using lentiviral delivery of control and *CHROME*-targeting shRNAs, we generated human hepatic HepG2 cell lines in which *CHROME* variants were constitutively knocked down (Fig. 3b), and performed RNA sequencing (RNA-Seq). Ingenuity Pathway Analysis of the RNA-Seq datasets identified lipid metabolism functions as among the top canonical pathways altered upon *CHROME* knockdown in HepG2 cells (Fig. 3c), most notably, the LXR pathway that regulates cellular responses to excess cholesterol, the farnesoid X receptor (FXR) pathway that regulates bile acid metabolism and cholesterol excretion, and the fatty acid β-oxidation pathway (Fig. 3c, Supplementary Fig. 6b, c).

CHROME post-transcriptionally regulates ABCA1 expression and cholesterol efflux

Activation of LXRs promotes cholesterol homeostasis through induction of a cadre of genes involved in cellular cholesterol efflux and reverse cholesterol transport. To investigate the

role of *CHROME* in LXR-mediated responses, we measured the ability of HepG2 cells expressing control and *CHROME*-targeting shRNAs to efflux cholesterol to apolipoprotein A1 (apoA-1), a process central to HDL biogenesis in the liver. Cholesterol efflux to exogenously supplied apoA1 was 50% lower in HepG2 cells expressing *CHROME* shRNAs compared to control shRNAs (Fig. 3d). To confirm our findings, we used a second method of *CHROME* depletion in primary human hepatocytes, in which we acutely knocked-down *CHROME* by transfecting GapmeR antisense oligonucleotides targeting a region of exon 1 common to all variants (Fig. 3e). Consistent with our findings using shRNAs, *CHROME* depletion in primary human hepatocytes using GapmeRs lowered cholesterol efflux to exogenous apoA-1 by approximately 50%, compared to control GapmeR treatment (Fig. 3f). We next measured the effects of *CHROME* on nascent HDL formation by primary human hepatocytes using ^{14}C-choline to label *de novo* synthesized phospholipids. Immunoprecipitation of apoA-1 secreted by primary human hepatocytes revealed 50% lower levels of apoA-1 lipidation in GapmeR-*CHROME* compared to GapmeR-control treated cells (Fig. 3g). By contrast, *CHROME* knockdown or overexpression in HepG2 cells did not alter the expression of genes involved in LDL uptake or cholesterol synthesis, nor were these processes altered upon manipulation of *CHROME* levels (Supplementary Fig 7a-e). As the ABCA1 transporter regulates cholesterol and phospholipid efflux to apoA-1, we next measured the effect of *CHROME* knockdown on ABCA1 protein and mRNA levels. We observed lower ABCA1 protein expression in GapmeR-*CHROME* compared to GapmeR-control treated hepatocytes (Fig. 3h, Supplementary Fig 7f). Using PCR primers to differentiate mature and unspliced mRNA transcripts[34] of *ABCA1*, we found that *CHROME* depletion reduced levels of mature, but not nascent *ABCA1* mRNA (Fig. 3i), suggesting a post-transcriptional mechanism.

CHROME localizes to P-bodies and associates with microRNAs

The cytoplasmic localization of *CHROME* raised the possibility that it may interact with cytosolic miRNAs known to post-transcriptionally regulate *ABCA1* expression and cholesterol efflux. To explore this potential mechanism, we used the miRTarget2 algorithm, which identified miR-33a, miR-33b, miR-27b and miR-128 as among the top miRNAs predicted to interact with *CHROME* (Supplementary Table 2). Using RNA hybrid analysis and manual curation, we found that *CHROME* variants harbor numerous putative binding sites for each of these miRNAs experimentally validated to regulate cholesterol efflux and/or HDL metabolism (Fig. 4a, Supplementary Fig. 8)[8,15,35,36]. Using RNAcofold, which takes into account the length and secondary structure of the transcripts, we calculated the free energy changes associated with the formation of *CHROME*-miRNA complexes and found that it predicted stable interactions of *CHROME* with miR-27b, miR-33a, miR-33b and miR-128, but not the control miRNA miR-16 (Fig. 4b). To first assess whether *CHROME* associates with miRNA complexes, we immunoprecipitated AGO2 from primary human hepatocytes and used qPCR to detect associated RNA, focusing on *CHROME-1*, *CHROME-3* and *CHROME-7* as these were the variants most regulated by cholesterol in monkeys. We found that *CHROME-1*, *CHROME-3* and *CHROME-7* transcripts were enriched in AGO2-immunoprecipitates compared to control IgG-precipitates (Fig. 4c). Similar association of *CHROME* variants with AGO2 was observed in THP-1 macrophages (Fig. 4c). To test whether *CHROME* binds specifically to miR-27b, miR-33a, miR-33b and

miR-128, we used MS2-tagged RNA affinity purification (MS2-TRAP)[37]. We cloned *CHROME-1*, *−3*, and *−7* upstream of MS2-binding sequences, and co-expressed these constructs in HEK293T cells with a YFP-tagged MS2-binding protein, which was used as bait to isolate MS2-tagged RNAs. qPCR analysis of RNAs co-precipitated with *CHROME*-MS2-binding protein complexes using anti-YFP antibody showed specific enrichment of miR-27b, miR-33a, miR-33b and miR-128 relative to control IgG, whereas no enrichment of control miRNAs (e.g., miR-16, miR-224 and miR-155) was detected (Fig. 4d).

To further investigate the association of *CHROME* with the RNA-Induced Silencing Complex (RISC), we performed RNA-FISH for *CHROME* in HEK293T cells that stably express AGO2-GFP. We observed colocalization of *CHROME* and AGO2 in puncta present in the cytoplasm (Fig. 4e). Notably, these puncta stained positive for enhancer of mRNA-decapping protein 4 (EDC4) (Fig. 4e), a marker of RNA processing bodies (P-bodies) that mediate miRNA sequestration or decay[38]. The presence of *CHROME* in P-bodies was confirmed by querying publicly available RNA-Seq data (ArrayExpress: E-MTAB-5477) of transcripts isolated from P-bodies purified from HEK293T cells using fluorescence-activated particle sorting[39]. *CHROME* was found to be significantly overrepresented in the P-body fraction when compared to the non-P-body fraction (adjusted P-value = 0.03; see Table S2 of [39]). Together, these data suggest that *CHROME* is localized to P-bodies, where it may sequester or degrade its miRNA binding partners. To investigate this possibility, we performed miRNA competition experiments with either wild type *CHROME-7* (*CHROME*^{WT}) or *CHROME-7* with mutated its miRNA binding sites mutated (*CHROME*^{MUT}). We transfected HEK293T cells with either *CHROME*^{WT} or *CHROME*^{MUT} and increasing amounts of control, miR-33a, miR-27b or miR-128 mimic. We found that cells expressing *CHROME*^{WT}, but not *CHROME*^{MUT}, had reduced levels of miR-33a, miR-27b and miR-128 compared to vector transfected cells. Because we controlled the concentration of miRNA molecules in this experiment by transfection, this suggests that *CHROME* can induce the decay of miR-33, miR-27b and miR-128 (Supplementary Fig. 9a).

CHROME modulates the actions of microRNAs known to repress cholesterol efflux and HDL biogenesis

To further investigate whether endogenous *CHROME* binding of miR-27b, miR-33a, miR-33b and miR-128 reduces the biological activities of these miRNAs, we assessed the effects of *CHROME* knockdown on those miRNAs' target gene networks using two unbiased approaches. First, we analyzed our RNA-Seq dataset of genes differentially expressed in shRNA-*CHROME* and shRNA-control expressing HepG2 cells by cumulative distribution function analysis to identify whether mRNAs targeted by miR-33a, miR-33b, miR-27b and miR-128 were selectively downregulated compared to non-target mRNAs. Indeed, we found significant overrepresentation of gene expression inhibition among miR-33a, miR-33b, miR-27b and miR-128 targets predicted by Targetscan, compared to non-target mRNAs (Fig. 4f). This is indicated in the cumulative distribution plot by a shift toward negative log2-fold changes in expression of targets (blue line) compared to non-targets (red line) (Fig. 4f). By contrast, mRNAs predicted to be targeted by miR-122, a control hepatic miRNA with known roles in lipid metabolism, showed no shift in log2-fold

changes in expression from non-target mRNAs, among genes differentially expressed in shRNA-*CHROME* and shRNA-control expressing HepG2 cells (Fig. 4f). To validate these findings, we used the bioinformatics tool miRHub to identify miRNAs that may act as regulatory hubs to control the genes differentially expressed in shRNA-*CHROME* and shRNA-control expressing HepG2 cells. miRHub predicts miRNA target sites in the 3'UTRs of differentially expressed genes and then determines by Monte Carlo simulation, for each miRNA, whether the number and strength of predicted targets is significantly greater than expected by chance. Using this unbiased approach, miR-27b and miR-128 were predicted to act as master regulators of genes significantly downregulated upon *CHROME* knockdown (Supplementary Fig. 9b), suggesting that these miRNAs' activities are increased in the absence of *CHROME*.

To experimentally test whether *CHROME* could alter cellular levels of its miRNA binding partners (miR-27b, miR-33a, miR-33b, miR-128) and their target mRNAs, we performed knockdown and overexpression experiments in hepatocytes. In primary human hepatocytes and HepG2 cells in which *CHROME* was depleted, using GapmeRs (Fig. 5a) or shRNA (Supplementary Fig. 9c), respectively, levels of miR-27b, miR-33a, miR-33b and miR-128 were higher than in cells treated with control GapmerRs or shRNAs. By contrast, no difference in levels of the control miRNA, miR-16, was observed in cells treated with control and *CHROME*-targeting GapmeRs or shRNAs (Fig. 5a, Supplementary Fig. 9c). Consistent with the increased levels of miR-27b, miR-33a, miR-33b and miR-128, we observed reduced levels of their common mRNA targets upon *CHROME* depletion by GapmeRs in primary human hepatocytes (Fig. 5b) or shRNA in HepG2 cells (Supplementary Fig. 9d), compared to control treatments. By contrast, we observed no difference in the mRNA levels of the control gene *ACTB* (Fig. 5b), or *PRKRA*, the gene adjacent to *CHROME* (Supplementary Data Fig. 9e). Conversely, overexpression of *CHROME-1*, *CHROME-3*, or *CHROME-7* by retroviral transduction of HepG2 cells reduced levels of miR-27b, miR-33a, miR-33b and miR-128 (Fig. 5c), and increased mRNA levels of their common target genes (Fig. 5d), compared to control vector-expressing HepG2 cells. Consistent with the shared ability of *CHROME*-targeted miRNAs to repress cholesterol efflux, we observed an increase in key genes in this pathway, including *ABCA1* and *OSBPL6* (Fig. 5d), and 2-fold higher levels of cholesterol efflux to apoA-1 (Fig. 5e),> when *CHROME* was overexpressed in HepG2 cells compared to control vector. No change in expression of *PRKRA*, the gene adjacent to *CHROME,* was observed when *CHROME* was overexpressed (Supplementary Fig. 9f).

To further investigate the relationship of *CHROME* with its miRNA binding partners and their target genes in humans, we obtained healthy hepatic tissue from 200 patients undergoing liver surgery and measured RNA levels by qPCR. Consistent with our *in vitro* findings, we found that levels of *CHROME* in the liver were inversely correlated with levels of miR-27b, miR-33a, miR-33b and miR-128, and positively correlated with levels of their target mRNAs (Fig. 5f). Furthermore, consistent with a role for *CHROME* in regulating hepatic cholesterol efflux to apoA-1, we found that hepatic expression of *CHROME-7* was positively and significantly correlated with plasma levels of HDL-C (Fig. 5g) and apoA-1 (Supplementary Fig. 9g).

CHROME regulates macrophage cholesterol efflux through non-coding RNA crosstalk

In addition to regulating hepatic HDL production, the efflux of excess cellular cholesterol is essential for maintaining homeostasis in peripheral tissues, particularly the artery wall, where macrophage cholesterol efflux protects from atherosclerotic plaque formation[2]. Given that *CHROME* was increased in cholesterol-loaded macrophages *in vitro* and in atherosclerotic plaques, we next tested the effects of *CHROME* loss-of-function in THP-1 macrophages. As we observed in hepatic cells, *CHROME*-GapmeR treated THP-1 macrophages showed lower *ABCA1* mRNA and protein levels compared to control GapmeR treated THP-1 macrophages (Fig. 6a, b, Supplementary Fig 10a), and this was associated with lower levels of cholesterol efflux to apoA-1 (Fig. 6c). Furthermore, GapmeR-depletion of *CHROME* in THP-1 macrophages increased levels of miR-27b, miR-33a, miR-33b, and miR-128, while decreasing levels of their target mRNAs (Supplementary Fig. 10b-d) relative to control GapmeR treatment, suggesting that *CHROME* acts via a similar mechanism in macrophages and hepatocytes to control cholesterol efflux. To directly test whether *CHROME*'s interactions with miRNAs mediate its effects on *ABCA1* expression, we assessed the ability of *CHROME-7*^{WT} and *CHROME-7*^{MUT}, in which the miRNA binding sites are mutated, to relieve miRNA-mediated repression of *ABCA1*. To do this, HEK293T cells were co-transfected with a human *ABCA1*-3' UTR luciferase reporter construct and either empty vector, *CHROME-7*^{WT} or *CHROME-7*^{MUT}, and then subsequently treated with miR-27b, miR-33a or control mimic. In control empty vector expressing cells, overexpression of miR-27b or miR-33a reduced *ABCA1*-3'UTR luciferase activity compared to control mimic, as expected (Fig. 6d). By contrast, miR-27b and miR-33a failed to repress *ABCA1*-3'UTR luciferase activity in *CHROME-7*^{WT} expressing cells (Fig. 6d). This protection required the miRNA response elements in *CHROME*, as miR-27b and miR-33a reduced *ABCA1*-3'UTR luciferase activity in *CHROME-7*^{MUT}-expressing cells to levels comparable to those observed in EV-transfected cells (Fig. 6d). Moreover, similar results were obtained using a 3'UTR-luciferase reporter construct for *OSBPL6* (Fig. 6e), which is another shared target of miR-27b and miR-33a/b that regulates cholesterol efflux. We then generated THP-1 cell lines expressing comparable levels of *CHROME-7*^{WT} or *CHROME-7*^{MUT}, or empty vector by retroviral transduction (Supplementary Fig. 10e). *Consistent* with the ability of *CHROME* to protect the *ABCA1*- and *OSBPL6*-3'UTRs from miRNA-mediated repression, THP-1-*CHROME-7*^{WT} macrophages showed higher levels of *ABCA1, OSBPL6* and *NPC1* mRNA (Fig. 6f), greater cholesterol efflux to apoA-1 (Fig. 6g) and reduced accumulation of cytoplasmic lipid droplets (Fig. 6h), as compared to THP-1^{EV} macrophages. These differences were associated with lower levels of miR-27b, miR-33a, miR-33b and miR-128 in THP-1-*CHROME-7*^{WT} than THP-1^{EV} macrophages (Fig. 6i), consistent with the ability of *CHROME* to functionally deplete these miRNAs. Notably, no differences in miR-27b, miR-33a, miR-33b or miR-128 levels, or *ABCA1*, *OSBPL6,* and *NPC1* expression, or cholesterol efflux and lipid droplet burden were observed between THP-1-*CHROME-7*^{MUT} and THP-1^{EV} macrophages (Fig. 6f-i). Collectively, these data suggest that *CHROME*'s capacity to regulate cellular cholesterol efflux and lipid droplet burden depend on interactions at its miRNA response elements.

Discussion

Our work identifies a novel primate-specific lncRNA, *CHROME*, that is increased in the setting of human atherosclerotic vascular disease and contributes to the regulation of cholesterol homeostasis. We find that *CHROME* levels are elevated in the plasma and arterial plaques of individuals with cardiovascular disease compared to healthy controls, and its expression is regulated in response to dietary and cellular cholesterol challenge. Mechanistic studies reveal a role for *CHROME* in the response of hepatocytes and macrophages to cholesterol overload, through the upregulation of cholesterol efflux and HDL biogenesis. *CHROME*'s expression is upregulated *in vitro* and *in vivo* by activation of the sterol-activated transcription factor LXR, which controls the expression of a cadre of genes involved in the response to cholesterol excess. Using gain- and loss-of-function studies, we establish that *CHROME* curbs the actions of the functionally related miRNAs, miR-27b, miR-33a, miR-33b and miR-128, to derepress their collective target genes, most notably those involved in cholesterol efflux and reverse cholesterol transport. This LXR-regulated mechanism enhances the cell's ability to respond to the changing environment by removing existing post-transcriptional "brakes" on cholesterol efflux, coincident with LXR-induced transcription of genes involved in the response to cholesterol excess. Together, our findings uncover an intricate interplay among non-coding RNA species in the fine tuning of cholesterol metabolism gene networks, and expand our understanding of the regulatory mechanisms that govern human cholesterol homeostasis in health and disease.

Many human lncRNAs exhibit low evolutionary conservation[40], as is the case for *CHROME*. Phylogenetic analyses suggest that *CHROME* emerged in the primate lineage (Supplementary Fig. 1b), and we did not detect shared synteny in other species (Supplementary Fig. 1c). Our studies in non-human primates show that *CHROME*'s expression is upregulated in the liver upon feeding a cholesterol-enriched diet or short-term treatment with an LXR agonist. Using primary human hepatocytes, we identify an important role for *CHROME* in the efflux of cholesterol and phospholipid to apoA1, processes that are critical to the production of nascent HDL particles. In a related process, we show that *CHROME* also regulates efflux of excess cholesterol from macrophages, which mediate the clearance of cholesterol-rich lipoproteins that can accumulate in tissues, such as the arterial wall. The primate-specificity of *CHROME* precludes *in vivo* studies of its effects on HDL metabolism and cholesterol efflux in typical preclinical animal models, such as mice. Nevertheless, loss-of-function studies in primary human hepatocytes reveal *CHROME*'s role in regulating HDL biogenesis, which support our observational data in a patient cohort showing a positive correlation of *CHROME* and plasma levels of HDL-C. Further testing of CHROME's ability to regulate reverse cholesterol transport *in vivo* will require loss-of-function studies in non-human primates.

Cholesterol levels in the cell, tissue and organism are dynamically controlled by a complex network of feedback mechanisms that maintain cholesterol homeostasis. In the last decade, studies have revealed the critical contributions of miRNAs in the post-transcriptional regulation of genes directing cholesterol homeostasis[6], and particularly, the cholesterol efflux pathway[41]. The *ABCA1* mRNA interacts with multiple miRNAs, including miR-20[42], miR-27b[11,14], miR-33a and miR-33b[7,8], miR-128[15], miR-144[12,13], miR-148[15], and which

collectively impart post-transcriptional repression of the ABCA1 transporter. Inhibition of those individual miRNAs *in vitro* using anti-sense oligonucleotides can increase ABCA1 protein and cholesterol efflux up to two-fold [7,8,11–15,42], and delivery of miR-33a/b[7,8,43–45], miR-128[15], or miR-144[12,13] inhibitors to mice or monkeys can raise plasma levels of HDL cholesterol by up to 50%. Thus, *CHROME*'s ability to simultaneously inhibit miR-27b, miR-33a, miR-33b and miR-128 provides a coordinated mechanism to relieve this potent post-transcriptional repression of the cholesterol efflux pathway. Furthermore, each variant of *CHROME* contains multiple binding sites for its interacting-miRNAs, which each repress multiple common target genes in lipid metabolism pathways, providing a mechanism for substantial regulatory crosstalk by *CHROME*. As levels of distinct miRNAs may vary by cell type and condition, *CHROME*'s ability to restrain the actions of a set of miRNAs with shared biological function allows for greater flexibility in the dynamic adjustment of cellular cholesterol efflux in discrete cell types, such as macrophages, enterocytes, and hepatocytes, which each express *ABCA1* and play distinct roles in reverse cholesterol transport and protection from atherosclerosis[46,47].

We show that *CHROME*'s interactions with miR-27b, miR-33a, miR-33b and miR-128 are central to its function in maintaining cholesterol homeostasis, as its ability to regulate the expression of *ABCA1*, cholesterol efflux and lipid droplet burden depend directly on the integrity of its binding sites for those miRNAs. Although the exact mechanisms by which *CHROME* titrates the availability of its miRNA binding partners remains unclear, our finding of *CHROME* in P-bodies opens the possibility that it traffics bound miRNAs to this granule for destabilization or degradation. miRNA-RISC complexes can have half-lives of days or more[48], thus *CHROME*-mediated compartmentalization of miRNAs in P-bodies could accelerate their turnover, or alternatively compromise their function through sequestration. Further studies will be needed to understand the spacio-temporal dynamics of *CHROME*'s associations with miRNAs, as well as other factors that may influence these interactions. For example, interactions of cytoplasmic lncRNAs and miRNAs are likely to be influenced by subcellular microenvironments that may increase local concentrations of RNAs and RNA binding proteins, as has been observed in neurons[49]. Furthermore, lncRNAs may interact with RNA binding proteins that may modify lncRNA stability, localization, and chemical (e.g., methylation) or secondary structure[50]. The identification of *CHROME,* and other lncRNAs of similar function, provides a gateway to begin to investigate the mechanisms underlying such interactions.

Our findings also reveal the expanding roles for non-coding RNAs in mediating crosstalk between the LXR and SREBP-2 transcription factors, which regulate opposing gene programs in the cholesterol overloaded and depleted states. Recent studies established that activation of LXR inhibits the expression of genes involved in cholesterol biosynthesis, including *SREBF2,* by upregulating the lncRNA *LeXis*, which sequesters the transcriptional co-factor RALY away from the promoters of cholesterol biosynthetic genes[23]. Conversely, we and others have shown that SREBP-2 represses the expression of genes involved in cholesterol efflux and reverse cholesterol transport by upregulating expression of miR-33a[7,8], which potently represses *ABCA1* and other genes contributing to cholesterol efflux and excretion (e.g., *OSBPL6*[9], *NPC1*[7,8], *ATG5*[51], *ABCB11*[10], *ATP8B1*[10]). The identification of *CHROME* as an LXR-regulated lncRNA that represses the actions of

miR-33a, expands this paradigm of reciprocal cross-talk between LXR and SREBP-2 mediated by non-coding RNAs. In addition, our RNA-Seq analyses suggest a role for *CHROME* in the regulation of fatty acid oxidation and the acute phase response in hepatocytes. As miR-33, miR-27b and miR-128 have been shown to repress genes regulating β-oxidation of fatty acids (e.g., *CROT*, *CPT1A*), *CHROME*'s interaction with these miRNAs is likely to underlie its effects on fatty acid oxidation. The mechanisms by which *CHROME* alters the acute phase response are less clear, and further studies will be needed to investigate *CHROME*'s role in the inflammatory response in hepatocytes and macrophages. Collectively, our data identify *CHROME* as a novel component of the multi-layered regulatory circuitry that is activated in response to cellular and systemic cholesterol overload, and unveil the regulatory crosstalk between non-coding RNAs that sustains cholesterol homeostasis in humans.

Methods

Human Studies.

All human studies complied with relevant ethical regulations. To assess the levels of *CHROME* RNA in individuals with coronary artery disease, we identified patient with established vascular disease in ongoing studies (NCT02106429 and NCT01897103)[52]. Plasma samples (coronary artery disease (CAD, n=14) or healthy control subjects (n=33)) were collected in accordance with the policies of New York University Langone Medical Center. All studies were approved by the NYULMC ethics committee. RNA was isolated from the plasma as described below. To measure *CHROME* expression in human healthy arterial and plaque atherosclerotic plaques, tissues and clinical data were obtained from patients undergoing surgery for stable or unstable carotid stenosis at the Department of Vascular Surgery, Karolinska University Hospital, Stockholm, Sweden, in collaboration with the Biobank of Karolinska Endarterectomies (BiKE) at the Centre for Molecular Medicine, Karolinska Institute. Gene expression analyses were performed in material obtained from individuals prospectively enrolled in the BiKE study between 2005 and 2008, total n=127 patient plaques and n=10 normal arteries (undiseased macroscopically atherosclerosis free-arteries, iliac and one aorta) were obtained from organ donors without any current or history of cardiovascular disease. No power calculation or selection of patients based on any other clinical criteria than symptomatic or asymptomatic carotid disease was done for this purpose; instead tissues were arrayed based on sample availability and RNA quality. All samples were collected with informed consent from patients, organ donors or their guardians. The BiKE study is approved by the Ethical Committee of Northern Stockholm with following ethical permits: EPN DNr 95– 276/277; DNr 02–146; DNr 02–147, DNr 2005/83–31; DNR 2009/512–31/2; 2012/619–32). The project is performed under the Swedish biobank regulations and prospective sampling is approved with informed consent procedure (DNr 2009/512–31/2). BiKE is registered at Socialstyrelsen (The National Board of Health and Welfare) and Biobank of Karolinska and approved by the Swedish Data Inspection Agency (approval date/number 2002–09-30 DNr 916–2002). The BiKE study cohort demographics, details of sample collection, processing and analyses have been previously described[53]. Gene expression profiles were analyzed by Affymetrix HG-U133 plus 2.0 Genechip microarrays. Robust multiarray average (RMA) normalization and

correction for batch effect was performed and processed gene expression data was returned in log2-scale. The microarray dataset is available from Gene Expression Omnibus (GSE21545). *In situ* hybridization of *CHROME* was performed on formalin-fixed samples of human carotid endarterectomy samples or iliac arteries as control tissues with LNA Detection Probes for *In Situ* Hybridization® (Exiqon) recognizing a sequence common to all *CHROME* variants (Supplementary Table 3) or control scramble-ISH custom LNA Detection Probe (Exiqon) at a final concentration 25 nM and labeled with DIG. To measure hepatic expression of *CHROME* and its miRNA targets, healthy liver tissue and serum samples were obtained from individuals undergoing liver surgery and experimental procedures were performed within the framework of the non-profit foundation HTCR Stiftung, including the informed patient's consent[54]. No power calculation or selection of patients based on any other clinical criteria other than undergoing liver surgery was done for this purpose; instead tissues were arrayed based on sample availability and RNA quality. This study was approved by the Ethics Committee of the Bavarian Medical Association (Bayerische Landesärztekammer) and the Ethics Committee of the Ludwig-Maximilians-University Munich. RNA (n=200) was isolated, and reverse transcribed (2 μg for mRNA; 1 μg for miRNA), and analyzed by qPCR as described below. Serum levels of apoA-1 and HDL cholesterol were determined using an immunoturbidimetric assay (Beckman Coulter, Krefeld, Germany) and an enzymatic assay (Beckman Coulter), respectively, and run on an AU5800 automated analyzer (Beckman Coulter).

Animal Studies.

Monkeys were housed in an AAALAC-accredited facility under the direct care of the Wake Forest University Health Sciences (WFUHS) Animal Resources Program. All experiments were approved by the WFUHS Institutional Animal Care and Use Committee (IACUC) and complied with relevant ethical regulations. Monkeys were singly housed in climate-controlled conditions with a 12 h light and dark cycle. Male African green (*Chlorocebus aethiops*) monkeys (n=5/group; age 4–9 years) maintained on a chow diet (0.002 mg/kcal cholesterol) were fed a high fat, moderate cholesterol (0.15 mg/kcal) diet for 8 weeks, and liver biopsies were obtained prior to and after diet feeding. For treatment with LXR agonist, adult male cynomolgus (*Macaca fascicularis*) monkeys (mean age 2.7 years) were fasted, anesthetized, and gavaged with either vehicle or 10 mg/kg GW3965 (n=5/group) daily for 2 days. Exactly 6 hr after dosing on day 2, fasted monkeys were euthanized and tissues were collected.

Cell Culture.

HEK293T, HepG2 and THP-1 cell lines were obtained from American Type Tissue Collection, authenticated using standard American Type Tissue Collection methods (morphology check by microscope, growth curve analysis) and tested monthly for mycoplasma contamination. HEK293T were maintained in high-glucose DMEM (Corning) supplemented with 10% fetal bovine serum (FBS, Life Technologies) and 1% penicillin/streptomycin (P/S, Life Technologies). HepG2 were maintained in EMEM (Corning) with 10% non-heat inactivated FBS and 1% P/S. THP-1 cells were maintained in RPMI 1640 (Corning) with 10% FBS and 1% P/S, and were differentiated into macrophages in the presence of 100 nM phorbol-12-myristate acetate (PMA, Sigma) for 48–72 h. Primary

human hepatocytes were obtained from Yecuris (Tualatin, OR), seeded on Coating Matrix (Life Technologies, #R011K) and maintained in HBM medium supplemented with HCM bullet kit (Lonza). To assess response to cholesterol loading and LXR activation, cells were stimulated with 37.5 μg/mL acetylated LDL (Biomedical Technologies) for 24 h, 10 μM T0901317 (Cayman Chemical Company) for 8 or 24 h, or 10 μg/mL cholesterol-cyclodextrin (Sigma) for 72 h. For transient knockdown of LXR in THP-1 cells, SMARTpool: ON-Targetplus siRNA against LXRα and LXRβ (Dharmacon, 25 nM each) was used for transfection. Non-targeting siRNA was used as control. For siLXR-studies, 48 h after transfection, cells were treated with 50 μg/mL acetylated LDL (acLDL) for 24 h.

RNA Isolation and qPCR.

Total RNA was isolated using TRIzol reagent (Invitrogen) and Direct-zol RNA MiniPrep columns (Zymo Research). RNA was reverse transcribed using iScript cDNA Synthesis Kit (Bio-Rad Laboratories), and quantitative PCR (qPCR) analysis was conducted using KAPA SYBR green Supermix (KAPA Biosystems) according to the manufacturer's instructions and quantified on a Mastercycler Realplex (Eppendorf). miRNA quantification was performed in quadruplicate with the miScript SYBR Green PCR Kit (Qiagen) using Qiagen miScript Primer Assays listed in Supplementary Table 3. Fold change in mRNA and miRNA expression was calculated using the comparative cycle method ($2^{-\Delta\Delta Ct}$) normalized to the housekeeping genes (*GAPDH* for mRNA; *U6* or miR-16 for miRNA), or μg of RNA (for tissue profiling). For plasma samples, RNA was isolated using TRIzol reagent (4:1 vol) followed by the RNA Clean & Concentrator-5 Plasma/Serum kit (Zymo Research). 5 μL of total RNA was reverse transcribed and used for qPCR. Copy numbers were determined using standard curves of *CHROME* variants.

Chromatin Immunoprecipitation Assay.

THP-1 cells differentiated with PMA were treated with 10 μM T0901317 for 8 h, and cells were treated with 1% formaldehyde to cross-link. The reaction was stopped with 0.125 M glycine, followed by washing in ice cold PBS, and the cells were pelleted. Nuclear lysates were collected and passed through a 25-gauge needle and sonicated until chromatin was sheared to 500–2000 bp fragments as previously described. For immunoprecipitation of LXR, 30 μg of chromatin was incubated with a cocktail of 3 μg LXRα and 3 μg LXRβ antibody (Abcam, #ab41902 and #ab56237) or isotype matched IgG (Abcam, #ab171870). Bound chromatin was immunoprecipitated using Dynabeads Protein G (Life Technologies) and bead/chromatin complexes were washed and dissociated at 65°C. DNA was purified using PrepEase DNA Clean-Up Kit (Affymetrix) and 1 μL of DNA was used for quantitative PCR.

RNA Fluorescence *In Situ* Hybridization

RNA fluorescence *in situ* hybridization and simultaneous RNA/DNA detection were performed as described[55,56]. Briefly, cells were fixed in 4% paraformaldehyde (PFA), permeabilized in CSK buffer, 5% triton X-100, and vanadyl ribonucleoside complex (VRC), and subsequently stored in PBS or 70% ethanol. DNA probes (1 μg/reaction) were nick-translated using biotin-11-dUTP or digoxigenin-16-dUTP (Roche Diagnostics). RNA-specific hybridization was carried out under non-denaturing conditions where the DNA was

not accessible. For colocalization with AGO2, HEK293T cells were transfected with AGO2-GFP plasmid (Addgene, #21981) for 24 h, and fluorescence in situ hybridization was performed for *CHROME* as described above, or cells were fixed in 4% PFA blocked/permeabilized in 2.5% BSA/0.1% Triton X-100, and stained for EDC4, cells using a rabbit anti-human EDC4 (Cell Signaling Technology, #2548) followed by fluorescent goat anti-rabbit secondary antibodies (Life Technologies, #A-11011).

Gain- and Loss-of-Function Studies.

For RNA interference studies, short hairpin RNAs (shRNA) targeting a region common to all *CHROME* variants or a non-targeting control shRNA (Supplementary Table 3) were cloned into the pLKO vector (Addgene, #8453) and transfected into HEK293T cells with packaging vectors psPAX2 (Addgene, #12260) and pMD2.G (Addgene, #12259). After 48 h, the culture media was isolated and used to transduce HepG2 cells. Cells stably expressing the shRNAs were selected using 5 μg/mL puromycin (Thermo Fisher Scientific). For transient knockdown of *CHROME*, primary human hepatocytes, HepG2 cells or PMA-differentiated THP-1 cells were transfected with 62.5 nM locked nucleic acid (LNA) GapmeRs targeting a common regions of all *CHROME* variants or Negative Control A (Exiqon) using Lipofectamine RNAiMax (Life Technologies). To create *CHROME*-overexpressing cell lines, *CHROME* cDNAs were obtained from Genscript and cloned into pMSCV-PIG vector (Addgene, #21654) and transfected into HEK293T cells with packaging vectors pCMV-VSV-G (Addgene, #8454) and pCMV-Gag-Pol (Cell Biolabs, #RV-111). After 48 h, the culture media was isolated and used to transduce THP-1 or HepG2 cells, and cells were selected using puromycin (5 μg/mL, Thermo Fisher Scientific). To mutate the predicted miR-27b, miR-33a, miR-33b and miR-128 binding sites within *CHROME-7*, we deleted the seed match sequence for those miRNAs with the Quickchange XL kit (Stratagene) using the primers indicated in Supplementary Table 3. *CHROME-7* mutant expressing cell lines were generated as described above. All constructs were confirmed by sequencing.

RNA-sequencing

RNA was isolated in triplicate from HepG2 cells expressing shRNA against all *CHROME* variants or control shRNA. RNA was used to generate barcoded cDNA libraries using the TruSeq RNA Sample Preparation kit (Illumina). Indexed libraries were pooled and sequenced (paired-end 50 or 100 bp reads) on the Illumina HiSEQ platform. RNA-seq reads were aligned using the STAR Aligner against hg19 annotations. Gene counting was done using featureCounts. Raw counts were normalized and DE-analysis was performed using DESeq2. RNA-Seq data are deposited in the Gene Expression Omnibus under the accession number GSE97469.

Bioinformatics.

The coding Potential of *CHROME* variants was predicted using the Coding Potential Calculator (CPC, http://cpc.cbi.pku.edu.cn/programs/cpc.do) and the Coding Potential Tool Assessment (CPAT, http://lilab.research.bcm.edu/cpat/calculator_sub.php) algorithms. Kozak strength was determined using the NCBI ORFFinder (http://atgpr.dbcls.jp/). LXRE sequence elements in the regulatory regions of *CHROME* were defined using JASPAR (http://

jaspar.genereg.net/). For calculations of the mean free energy changes associated with the formation of CHROME-miRNA complexes were calculated using RNAcofold (http://rna.tbi.univie.ac.at/cgi-bin/RNAWebSuite/RNAcofold.cgi), which predicts secondary structures of single stranded RNA sequences upon dimer formation This algorithm takes into account the length of the transcript and secondary structure. One thousand randomly selected sections of the human genome of length 21–22 nucleotides long were run through RNAcofold, along with annotated miRNA sequences including miR-27b, miR-128, miR-33a, miR-33b and miR-16 and aligned pairwise with *CHROME* transcripts. For RNA-Seq analyses, Ingenuity Pathway Analysis (Qiagen) was used to evaluate the most significantly altered genes and pathways. Cumulative distribution function analysis was performed using the statistical software package R 2.8.0 (www.r-project.org)[57] for predicted targets of miRNA-27b, miR-33a/b, miR-128, and miR-122 versus non-targets (defined using Targetscan; http://www.targetscan.org/vert_72/). Statistical enrichment of predicted miR-33a/b, miR-27b and miR-128 target sites among differentially regulated genes in HepG2 RNA-Seq datasets was performed using miRhub as described[58].

Western Blots

Protein was extracted in RIPA buffer (Cell Signaling) with protease and phosphatase inhibitors (Roche) and subsequently normalized by Pierce BCA Protein Assay Kit (Thermo Fisher Scientific). Samples (30 μg/well) were electrophoresed on 4–20% TGX-gradient gels (Bio-Rad Laboratories) and transferred to nitrocellulose membranes at 125 V for 2 h. Membranes were incubated overnight with specified antibodies directed against ABCA1 (Novus Biologicals, NB400–105) and HSP90 (BD Biosciences, #610419). Proteins were visualized using appropriate secondary antibodies and scanned using the Odyssey Imaging System (Li-Cor Biosciences). Quantification was performed using Image Studio software (Li-Cor Biosciences).

Cholesterol Efflux Assay and Neutral Lipid Staining.

For cholesterol efflux assays, HepG2 or THP-1 cells stably expressing *CHROME* variants were seeded in 24-well plates at a density of 1×10^6 cells, and THP-1 cells were treated with PMA as described above. Primary hepatocytes were seeded at 2×10^5 in 48-wells plates and transfected with control or *CHROME*-targeting GapmeRs. Cells were labeled with 0.5 μCi/mL of ^{3}H-cholesterol (PerkinElmer) for 24 h, washed twice with PBS and then incubated with 2 mg/mL fatty-acid free BSA (FAFA, Sigma-Aldrich) in media for 24 h. To induce efflux, 50 μg/mL human apoA-1 in FAFA media was added and supernatants were collected after 8 or 24 h. ApoA-1 dependent efflux was expressed as a percentage of total cell ^{3}H-cholesterol content. To visualize neutral lipids, THP-1 cells stably expressing *CHROME* variants were treated with PMA as described above and then incubated with 37.5 μg/mL acetylated LDL for 24 h. Cells were then stained using Nile Red (Thermo Fisher Scientific) as previously described[59].

Endogenous apoA-1 Lipidation.

To assess phospholipid efflux to endogenous apoA-1 in primary human hepatocytes, cells were seeded at 2×10^5 in 48-wells plates and transfected with GapmeRs as described above. Hepatocytes were labeled with 5 μCi/mL of ^{14}C-choline chloride (PerkinElmer) for 48 h,

washed twice and incubated for 24 h in serum-free HCM supplemented with 10 μM T0901317 (Cayman Chemical Company). ApoA-1 secreted into the cell culture supernatant was immunoprecipitated from the culture medium with polyclonal anti-human apoA-1 (EMD Millipore, #178422) and protein G-sepharose (Sigma-Aldrich), washed in PBS, and scintillation counting was performed to assess amount of phospholipid efflux.

Immunoprecipitation of AGO2.

Argonaute-2 (AGO2) was immunoprecipitated from primary human hepatocytes or PMA differentiated THP-1 macrophages using the MagnaRIP RNA-Binding Protein Immunoprecipitation Kit (EMD Millipore) according to the manufacturers' instructions. Briefly, an antibody targeting human AGO2 (Millipore, RIPAb+ #03–110) or an isotype matched control antibody (EMD Millipore, #CS200621) were bound to magnetic beads and incubated with lysed cells at 4°C for 24 h. Beads were isolated and coprecipitated RNA was purified, cleaved from AGO2 by proteinase K, and purified using TRIzol reagent. PCR analysis of total RNA was performed to detect *CHROME*, and enrichment of *CHROME* variants in the AGO2 fraction was determined by correcting for both *GAPDH* levels and the fraction that coprecipitated with IgG antibodies.

MS2-tagged RNA Affinity Purification.

MS2-tagged RNA affinity purification (MS2-TRAP) was performed as previously described[37]. Briefly, HEK293T cells were transfected with plasmids expressing *CHROME-1*, *CHROME-3*, or *CHROME-7* in frame with an MS2 binding sequence, together with a plasmid expressing YFP-tagged MS2 binding protein for 24 h. MS2 binding protein was immunoprecipitation using an antibody against GFP (Roche Diagnostics, #118144600001) or isotype matched IgG control antibody (EMD Millipore, #CS200621), and coprecipitated RNA was isolated using Trizol. Total RNA was analyzed by qPCR for miR-16, miR-27b, miR-33a/b, miR-128, miR-155, miR-224 and *U6*. Enrichment of miRNAs bound to *CHROME* was determined by correcting for *U6* levels, the fraction that coprecipitated with IgG antibodies and the expression levels of miRNAs for the empty control.

Cholesterol Biosynthesis and LDL Uptake.

HepG2 cells were seeded and incubated with 5 μCi/mL of ^{3}H-acetate (Amersham) in EMEM supplemented with 10% LPDS. After 24 h, cells were lysed with 0.25N NaOH and lipid extraction was performed as described[60]. The organic layer was dried under N_2 gas and samples were resuspended in hexane. Lipids were separated by thin layer chromatography in the solvent system hexane:diethyl ether:acetic acid (105:45:1). The bands corresponding to cholesterol fractions were collected and radioactivity was determined by liquid scintillation counting. Data were normalized to cellular protein levels obtained by Pierce BCA Protein Assay Kit. To measure LDL uptake, HepG2 cells were seeded in poly-D-lysine coated Labtek slides and incubated for 4 h with Dil-LDL (10 μg/mL, AlfaAesar) in EMEM supplemented with 2 mg/mL BSA. Intracellular LDL was detected by microscopy (Leica SP5) and fluorescence intensity was quantified using Fiji software (http://www.fiji.com) from 6 fields-of-view.

microRNA Degradation.

HEK293T cells were co-transfected with wild-type or mutant *CHROME*-7 plasmid and miRNA mimics at various concentration (25 nm, 50 nm, 100 nm) with Lipofectamine 2000 (Invitrogen) overnight. miRNA expression was quantified by qPCR. Control non-targeting mimic and empty vector (EV) were used for normalization.

3'UTR Luciferase Experiments.

Human *ABCA1*- and human *OSBPL6*-3'UTR luciferase/renilla reporter constructs were obtained from GeneCopoeia. HEK293T cells were cotransfected with 1 μg of 3'UTR luciferase reporter vector and wild-type or mutant *CHROME* plasmid. Cells were then treated with 50 nM miRNA mimic or control mimic using Lipofectamine 2000 (Invitrogen) in a 96-well plate. 3'UTR activity was assessed by measuring luciferase using the Dual Glo Luciferase Assay System (Promega). Firefly luciferase activity was normalized to renilla luciferase activity.

Statistics.

The statistical significance of differences of 3 or more independent biological replicates was evaluated with the Student's t test or two-way analysis of variance (ANOVA) for multiple group comparisons. The Tukey and Dunnett tests were used as follow-up tests to the ANOVAs, where the Tukey test was used to compare every mean with every other mean, and the Dunnett test was used when comparing every mean to a control mean. For human liver gene expression studies, data were quantile normalized using the statistical software package R 2.8.0[57]. Normality of distribution was tested using the Kolmogorov-Smirnov test implemented in the PRISM statistical software (GraphPad). No significant effects of age and sex on gene expression levels were detected. Spearman correlation coefficients between gene expression data and serum apoA-1 and HDL cholesterol levels and levels of significance were calculated using the SAS statistic software (SAS Version 9.3, SAS Institute, Inc.).

Supplementary Material

Refer to Web version on PubMed Central for supplementary material.

Acknowledgements:

This work was supported by grants from the NIH [R01HL119047 (KJM), R35HL135799 (KJM), R01HL117226 (MJG), T32HL098129 (EJH, CvS), R01HL114978 (JSB), R00HL088528 (RET), R01HL111932 (RET), R01HL128996 (KCV), P01HL116263 (KCV), R01DK105965 (PS)], American Heart Association [14POST20180018 (CvS), 13CRP14410042 (JSB)], FINOVI (EPR), the Swedish Society for Medical Research (LPM) and the Heart and Lung Foundation (LPM), the German Research Foundation CRC 1123 Project B1 (DT, LMH), German Biobank Alliance BMBF 01EY1711C (German Ministry of Education and Research to DT and LMH) and Leducq Foundation CAD genomics (DT, LMH). The BiKE study was supported by the Swedish Heart and Lung Foundation, the Swedish Research Council (K2009–65X-2233–01-3, K2013–65X-06816–30-4, 349–2007-8703), Uppdrag Besegra Stroke (P581/2011–123), the Strategic Cardiovascular Programs of Karolinska Institutet and Stockholm County Council, the Foundation for Strategic Research and the European Commission (CarTarDis, AtheroRemo, VIA, AtheroFlux projects). We would like to thank E.A. Fisher (New York University) for helpful discussions, S. Zhao and Q. Sheng (Vanderbilt University) for their efforts in Seq-data analysis.

REFERENCES

1. Goedeke L & Fernandez-Hernando C Regulation of cholesterol homeostasis. Cell Mol Life Sci 69, 915–930 (2012). [PubMed: 22009455]
2. Siddiqi HK, Kiss D & Rader D HDL-cholesterol and cardiovascular disease: rethinking our approach. Curr Opin Cardiol 30, 536–542 (2015). [PubMed: 26192490]
3. Lee SD & Tontonoz P Liver X receptors at the intersection of lipid metabolism and atherogenesis. Atherosclerosis 242, 29–36 (2015). [PubMed: 26164157]
4. Scacalossi KR, van Solingen C & Moore KJ Long non-coding RNAs regulating macrophage functions in homeostasis and disease. Vascul Pharmacol (2018).
5. van Solingen C, Scacalossi KR & Moore KJ Long noncoding RNAs in lipid metabolism. Curr Opin Lipidol 29, 224–232 (2018). [PubMed: 29553997]
6. Feinberg MW & Moore KJ MicroRNA Regulation of Atherosclerosis. Circ Res 118, 703–720 (2016). [PubMed: 26892968]
7. Najafi-Shoushtari SH, et al. MicroRNA-33 and the SREBP host genes cooperate to control cholesterol homeostasis. Science 328, 1566–1569 (2010). [PubMed: 20466882]
8. Rayner KJ, et al. MiR-33 contributes to the regulation of cholesterol homeostasis. Science 328, 1570–1573 (2010). [PubMed: 20466885]
9. Ouimet M, et al. miRNA Targeting of Oxysterol-Binding Protein-Like 6 Regulates Cholesterol Trafficking and Efflux. Arterioscler Thromb Vasc Biol 36, 942–951 (2016). [PubMed: 26941018]
10. Allen RM, et al. miR-33 controls the expression of biliary transporters, and mediates statin- and diet-induced hepatotoxicity. EMBO Mol Med 4, 882–895 (2012). [PubMed: 22767443]
11. Goedeke L, et al. miR-27b inhibits LDLR and ABCA1 expression but does not influence plasma and hepatic lipid levels in mice. Atherosclerosis 243, 499–509 (2015). [PubMed: 26520906]
12. de Aguiar Vallim TQ, et al. MicroRNA-144 regulates hepatic ATP binding cassette transporter A1 and plasma high-density lipoprotein after activation of the nuclear receptor farnesoid X receptor. Circ Res 112, 1602–1612 (2013). [PubMed: 23519696]
13. Ramirez CM, et al. Control of cholesterol metabolism and plasma high-density lipoprotein levels by microRNA-144. Circ Res 112, 1592–1601 (2013). [PubMed: 23519695]
14. Liu XH, et al. Lnc RNA HOTAIR functions as a competing endogenous RNA to regulate HER2 expression by sponging miR-331–3p in gastric cancer. Mol Cancer 13, 92 (2014). [PubMed: 24775712]
15. Wagschal A, et al. Genome-wide identification of microRNAs regulating cholesterol and triglyceride homeostasis. Nat Med 21, 1290–1297 (2015). [PubMed: 26501192]
16. Quinn JJ & Chang HY Unique features of long non-coding RNA biogenesis and function. Nat Rev Genet 17, 47–62 (2016). [PubMed: 26666209]
17. Palazzo AF & Lee ES Non-coding RNA: what is functional and what is junk? Front Genet 6, 2 (2015). [PubMed: 25674102]
18. Schmitz SU, Grote P & Herrmann BG Mechanisms of long noncoding RNA function in development and disease. Cell Mol Life Sci 73, 2491–2509 (2016). [PubMed: 27007508]
19. Freedman JE, Miano JM, National Heart L & Blood Institute Workshop P Challenges and Opportunities in Linking Long Noncoding RNAs to Cardiovascular, Lung, and Blood Diseases. Arterioscler Thromb Vasc Biol 37, 21–25 (2017). [PubMed: 27856459]
20. Yan C, Chen J & Chen N Long noncoding RNA MALAT1 promotes hepatic steatosis and insulin resistance by increasing nuclear SREBP-1c protein stability. Sci Rep 6, 22640 (2016). [PubMed: 26935028]
21. Liu C, et al. Long noncoding RNA H19 interacts with polypyrimidine tract-binding protein 1 to reprogram hepatic lipid homeostasis. Hepatology 67, 1768–1783 (2018). [PubMed: 29140550]
22. Li D, et al. Identification of a novel human long non-coding RNA that regulates hepatic lipid metabolism by inhibiting SREBP-1c. Int J Biol Sci 13, 349–357 (2017). [PubMed: 28367099]
23. Sallam T, et al. Feedback modulation of cholesterol metabolism by the lipid-responsive non-coding RNA LeXis. Nature 534, 124–128 (2016). [PubMed: 27251289]

24. Sallam T, et al. Transcriptional regulation of macrophage cholesterol efflux and atherogenesis by a long noncoding RNA. Nat Med 24, 304–312 (2018). [PubMed: 29431742]
25. Pasmant E, Sabbagh A, Vidaud M & Bieche I ANRIL, a long, noncoding RNA, is an unexpected major hotspot in GWAS. FASEB J 25, 444–448 (2011). [PubMed: 20956613]
26. Holdt LM & Teupser D Recent studies of the human chromosome 9p21 locus, which is associated with atherosclerosis in human populations. Arterioscler Thromb Vasc Biol 32, 196–206 (2012). [PubMed: 22258902]
27. Nsengimana J, et al. Enhanced linkage of a locus on chromosome 2 to premature coronary artery disease in the absence of hypercholesterolemia. European journal of human genetics : EJHG 15, 313–319 (2007). [PubMed: 17149386]
28. North KE, Martin LJ, Dyer T, Comuzzie AG & Williams JT HDL cholesterol in females in the Framingham Heart Study is linked to a region of chromosome 2q. BMC genetics 4 Suppl 1, S98 (2003). [PubMed: 14975166]
29. Kapusta A, et al. Transposable elements are major contributors to the origin, diversification, and regulation of vertebrate long noncoding RNAs. PLoS Genet 9, e1003470 (2013). [PubMed: 23637635]
30. Perisic L, et al. Profiling of atherosclerotic lesions by gene and tissue microarrays reveals PCSK6 as a novel protease in unstable carotid atherosclerosis. Arterioscler Thromb Vasc Biol 33, 2432–2443 (2013). [PubMed: 23908247]
31. Moore KJ & Tabas I Macrophages in the pathogenesis of atherosclerosis. Cell 145, 341–355 (2011). [PubMed: 21529710]
32. Cabili MN, et al. Localization and abundance analysis of human lncRNAs at single-cell and single-molecule resolution. Genome Biol 16, 20 (2015). [PubMed: 25630241]
33. Lennox KA & Behlke MA Cellular localization of long non-coding RNAs affects silencing by RNAi more than by antisense oligonucleotides. Nucleic Acids Res 44, 863–877 (2016). [PubMed: 26578588]
34. John S, et al. Kinetic complexity of the global response to glucocorticoid receptor action. Endocrinology 150, 1766–1774 (2009). [PubMed: 19131569]
35. Davalos A, et al. miR-33a/b contribute to the regulation of fatty acid metabolism and insulin signaling. Proceedings of the National Academy of Sciences of the United States of America 108, 9232–9237 (2011). [PubMed: 21576456]
36. Vickers KC, et al. MicroRNA-27b is a regulatory hub in lipid metabolism and is altered in dyslipidemia. Hepatology 57, 533–542 (2013). [PubMed: 22777896]
37. Yoon JH, Srikantan S & Gorospe M MS2-TRAP (MS2-tagged RNA affinity purification): tagging RNA to identify associated miRNAs. Methods 58, 81–87 (2012). [PubMed: 22813890]
38. Liu J, Valencia-Sanchez MA, Hannon GJ & Parker R MicroRNA-dependent localization of targeted mRNAs to mammalian P-bodies. Nat Cell Biol 7, 719–723 (2005). [PubMed: 15937477]
39. Hubstenberger A, et al. P-Body Purification Reveals the Condensation of Repressed mRNA Regulons. Mol Cell 68, 144–157 e145 (2017). [PubMed: 28965817]
40. Ulitsky I Evolution to the rescue: using comparative genomics to understand long non-coding RNAs. Nat Rev Genet 17, 601–614 (2016). [PubMed: 27573374]
41. Rayner KJ & Moore KJ MicroRNA control of high-density lipoprotein metabolism and function. Circ Res 114, 183–192 (2014). [PubMed: 24385511]
42. Liang B, et al. MicroRNA-20a/b regulates cholesterol efflux through post-transcriptional repression of ATP-binding cassette transporter A1. Biochim Biophys Acta 1862, 929–938 (2017).
43. Marquart TJ, Allen RM, Ory DS & Baldan A miR-33 links SREBP-2 induction to repression of sterol transporters. Proceedings of the National Academy of Sciences of the United States of America 107, 12228–12232 (2010). [PubMed: 20566875]
44. Rayner KJ, et al. Inhibition of miR-33a/b in non-human primates raises plasma HDL and lowers VLDL triglycerides. Nature 478, 404–407 (2011). [PubMed: 22012398]
45. Rayner KJ, et al. Antagonism of miR-33 in mice promotes reverse cholesterol transport and regression of atherosclerosis. J Clin Invest 121, 2921–2931 (2011). [PubMed: 21646721]

46. Abumrad NA & Davidson NO Role of the gut in lipid homeostasis. Physiol Rev 92, 1061–1085 (2012). [PubMed: 22811425]

47. Westerterp M, et al. ATP-binding cassette transporters, atherosclerosis, and inflammation. Circ Res 114, 157–170 (2014). [PubMed: 24385509]

48. Ameres SL, et al. Target RNA-directed trimming and tailing of small silencing RNAs. Science 328, 1534–1539 (2010). [PubMed: 20558712]

49. Cajigas IJ, et al. The local transcriptome in the synaptic neuropil revealed by deep sequencing and high-resolution imaging. Neuron 74, 453–466 (2012). [PubMed: 22578497]

50. Jens M & Rajewsky N Competition between target sites of regulators shapes post-transcriptional gene regulation. Nat Rev Genet 16, 113–126 (2015). [PubMed: 25488579]

51. Ouimet M, et al. microRNA-33 Regulates Macrophage Autophagy in Atherosclerosis. Arterioscler Thromb Vasc Biol 37, 1058–1067 (2017). [PubMed: 28428217]

METHODS ONLY REFERENCES

52. Montenont E, et al. Platelet WDR1 suppresses platelet activity and associates with cardiovascular disease. Blood (2016).

53. Perisic L, et al. Gene expression signatures, pathways and networks in carotid atherosclerosis. J Intern Med 279, 293–308 (2016). [PubMed: 26620734]

54. Thasler WE, et al. Charitable State-Controlled Foundation Human Tissue and Cell Research: Ethic and Legal Aspects in the Supply of Surgically Removed Human Tissue For Research in the Academic and Commercial Sector in Germany. Cell and tissue banking 4, 49–56 (2003). [PubMed: 15256870]

55. Johnson CV, Singer RH & Lawrence JB Fluorescent detection of nuclear RNA and DNA: implications for genome organization. Methods in cell biology 35, 73–99 (1991). [PubMed: 1723481]

56. Tam R, Smith KP & Lawrence JB The 4q subtelomere harboring the FSHD locus is specifically anchored with peripheral heterochromatin unlike most human telomeres. The Journal of cell biology 167, 269–279 (2004). [PubMed: 15504910]

57. Ihaka R.a.G.R A Language for Data Analysis and Graphics. Journal of Computational and Graphical Statistics 5, 299–314 (1996).

58. Baran-Gale J, Fannin EE, Kurtz CL & Sethupathy P Beta cell 5'-shifted isomiRs are candidate regulatory hubs in type 2 diabetes. PLoS One 8, e73240 (2013). [PubMed: 24039891]

59. Listenberger LL & Brown DA Fluorescent detection of lipid droplets and associated proteins. Curr Protoc Cell Biol **Chapter** 24, Unit 24 22 (2007).**Chapter**

60. Folch J, Lees M & Sloane Stanley GH A simple method for the isolation and purification of total lipides from animal tissues. J Biol Chem 226, 497–509 (1957). [PubMed: 13428781]

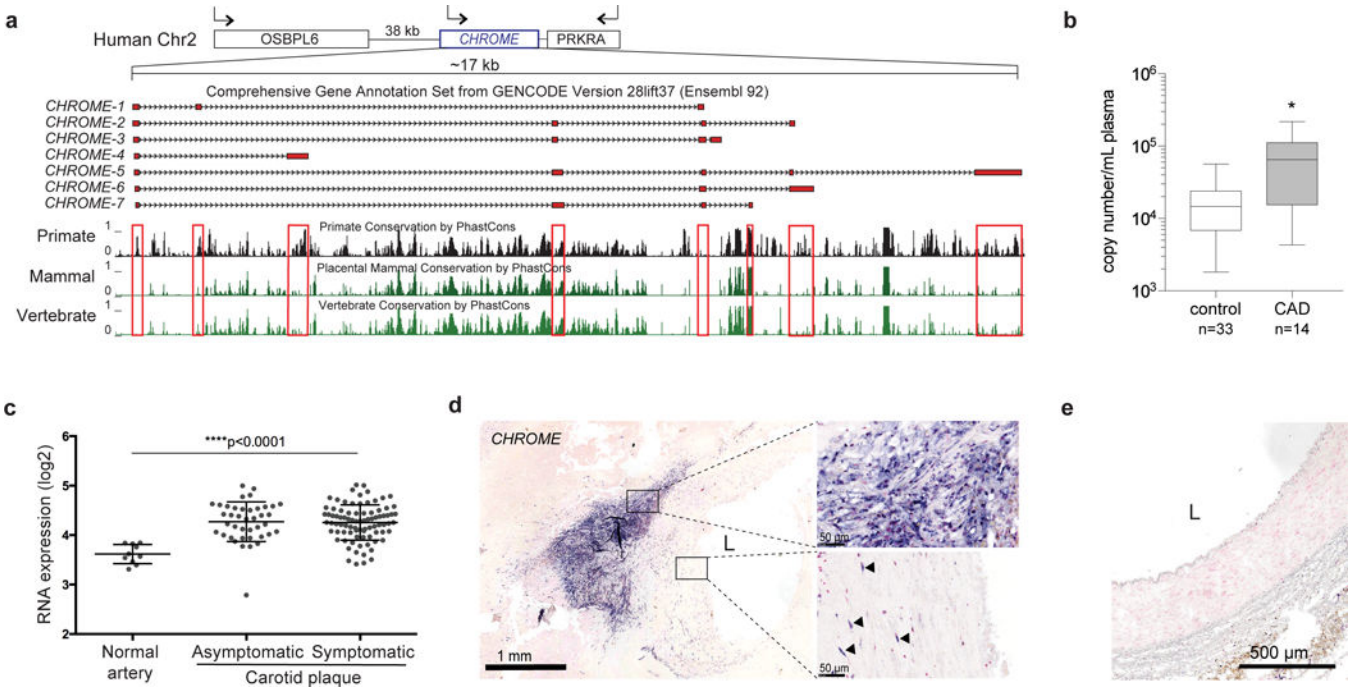

Figure 1. Levels of lncRNA *CHROME* are increased in atherosclerotic cardiovascular disease.

a, Schematic representation of the human *CHROME* locus, which encodes seven splice variants (*CHROME1–7*). PhastCons analysis showing the conservation of *CHROME* in primates but not in other mammals or vertebrates. Red boxes indicate exonic sequences. **b,** Box and whiskers plot depicting plasma levels of *CHROME* RNA in individuals with coronary artery disease (CAD, n=14) or healthy control subjects (n=33). Box represents 25th to 75th percentiles, with line in middle indicating the median. **c,** *CHROME* expression in normal artery (n=10), or carotid endarterectomy plaques from individuals with asymptomatic (n=40) or symptomatic (n=77) carotid stenosis. Data are the mean ± SEM. **d-e,** Detection of *CHROME* RNA (purple) by *in situ* hybridization of human (d) carotid plaque and (e) control iliac artery. Sections were counterstained with nuclear fast red to visualize nuclei (pink). Boxed regions in (d) indicate *CHROME* expression in areas of inflammatory cell infiltrate (top) and in the neointima (bottom, arrowheads). Lumen (L). Data are representative of staining from 8 independent plaques. P-values were calculated using (**b**) a Mann-Whitney test, and (**c**) two-way ANOVA, *P≤0.05, ****P≤0.0001.

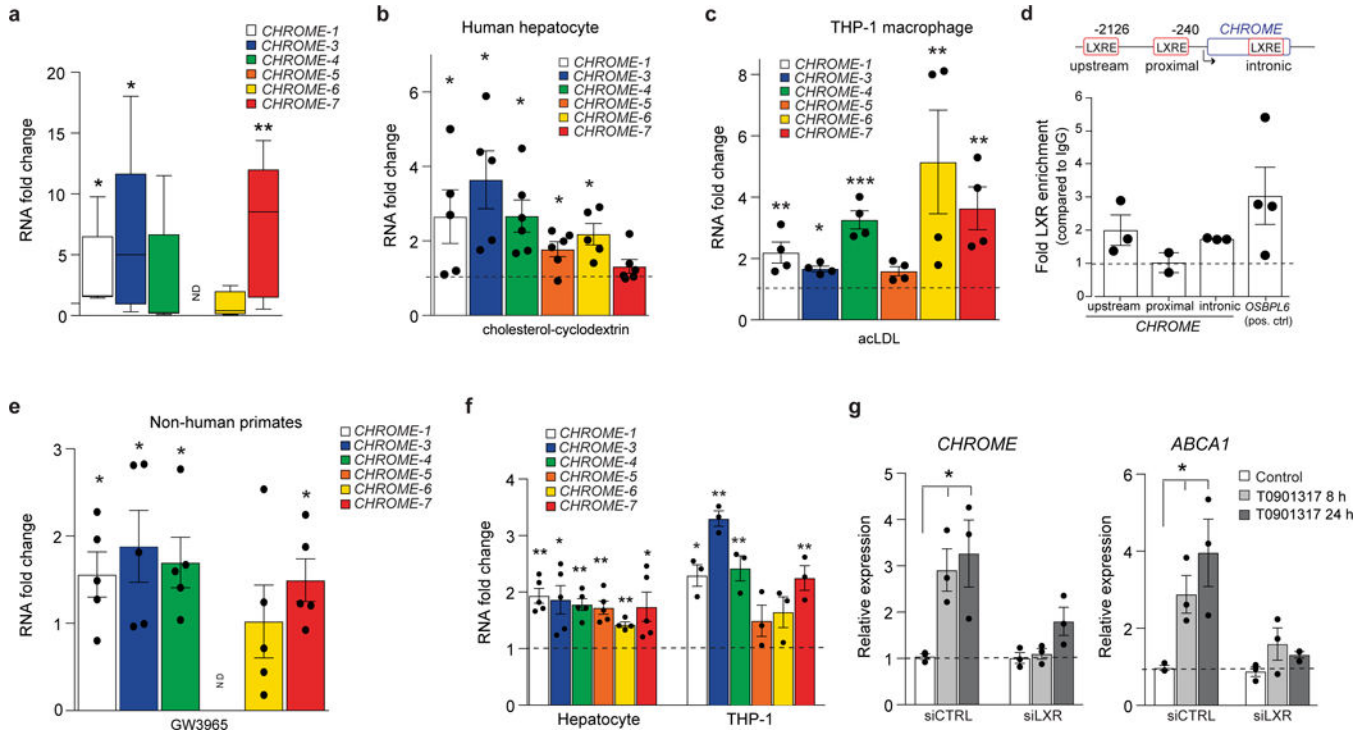

Figure 2. LncRNA *CHROME* is regulated by dietary and cellular cholesterol via the LXR-transcription factor.

a, qPCR analysis of *CHROME* variant expression in (a) livers of African green monkeys (n=5/group) before fed a high fat moderate cholesterol diet (8 weeks) compared to baseline chow diet. Box represents 25th to 75th percentiles, with line in middle indicating the median. **b-c**, qPCR analysis of *CHROME* variant expression in (b) human HepG2 cells treated with cholesterol-cyclodextrin (10 μg/mL; 72 h) compared to vehicle, and (c) human THP-1 macrophages treated with acetylated LDL (37.5 μg/mL, 24 h) compared to untreated. Data are the mean ± SEM of 5 (b) and 4 (c) independent experiments. **d,** Schematic diagram of predicted LXR response elements (LXRE) in the *CHROME* locus (top) and relative enrichment of *CHROME* in LXRα/β chromatin immunoprecipitates from THP-1 cells treated with LXR agonist (T0901317, 10 μM) at each of the predicted sites. Enrichment of LXR at *OSBPL6* locus is shown as positive control. Data are normalized to IgG control. **e,** qPCR analysis of *CHROME* variant expression in livers of male cynomolgus monkeys treated with LXR agonist (GW3965) or vehicle for 2 days. Data are the mean ± SEM of 5 monkeys/group. **f**, qPCR analysis of *CHROME* variant expression in primary human hepatocytes and THP-1 macrophages treated with LXR agonist (10 μM T0901317) relative to vehicle control. Data are the mean ± SEM of 3–5 independent experiments. **g,** qPCR quantification of *CHROME* (all variants) and *ABCA1* mRNA in THP-1 macrophages transfected with an LXRα/β-targeting or control siRNA for 24 h and then treated with LXR agonist (10 μM T0901317). Data are the mean ± SEM of 3 biological replicates from a single experiment that is representative of 3 experiments. P-values were calculated using (**b, c, f, g**) two-tailed student's t-test and (**a, e**) two-way ANOVA. *P≤0.05, **P≤0.01, ***P≤0.001.

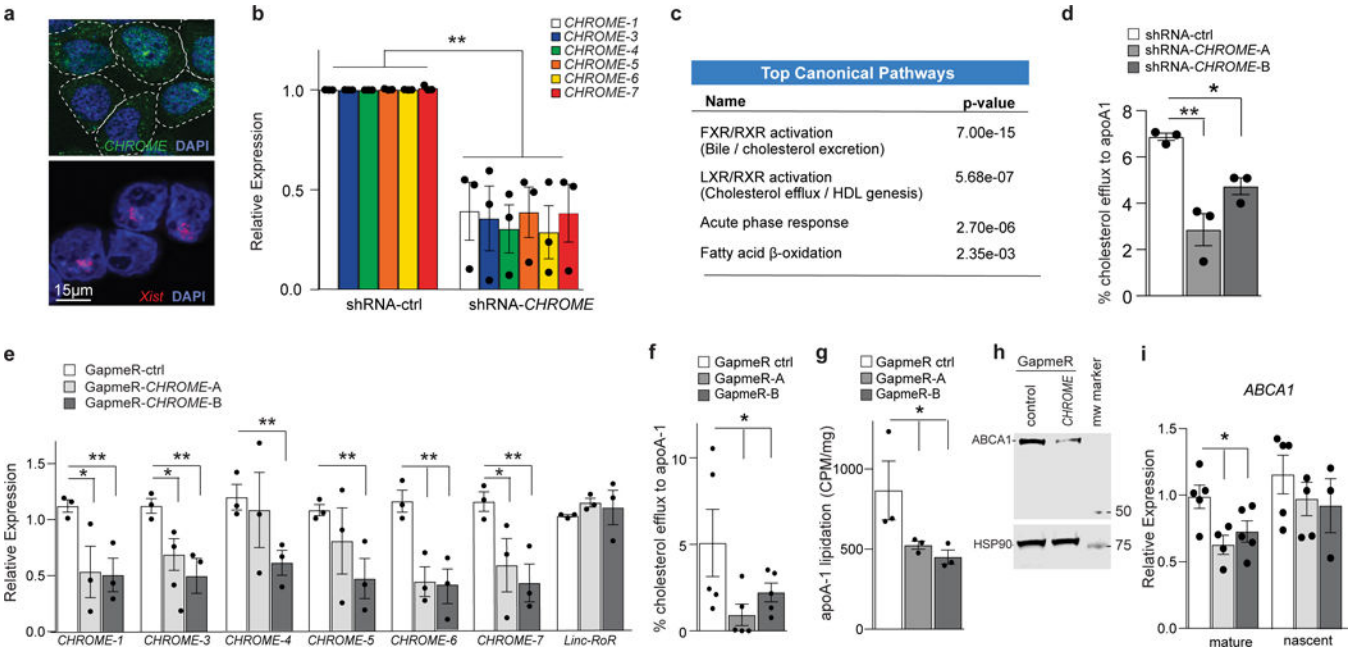

Figure 3. *CHROME* depletion in hepatocytes reduces cholesterol efflux and formation of nascent HDL particles.

a, Fluorescence *in situ* hybridization for *CHROME* (green) and *Xist* (red) RNA in HEK293T cells stained with DAPI to visualize nuclear DNA (blue). **b,** qPCR analysis of *CHROME* variants in HepG2 cells stably expressing an shRNA targeting all *CHROME* variants (shRNA-*CHROME*) or control shRNA (shRNA-ctrl). **c,** Ingenuity pathway analysis of RNA-Seq data from shRNA-*CHROME* and shRNA-ctrl expressing HepG2 cells showing the top canonical pathways altered upon *CHROME* knockdown. **d,** Measurement of cholesterol efflux to exogenous apoA-1 in HepG2 cells expressing shRNA-*CHROME* or shRNA-ctrl. **e,** qPCR quantification of *CHROME* variants in primary human hepatocytes transfected with control (GapmeR-ctrl) or *CHROME*-targeting GapmeRs (GapmeR-*CHROME*-A or GapmeR-*CHROME*-B)**. f,** Measurement of cholesterol efflux to exogenous apoA-1 in primary human hepatocytes transfected with control or *CHROME*-targeting GapmeRs. **g,** Measurement of phospholipid efflux to apoA1 secreted from primary human hepatocytes labelled with C^{14}-choline chloride and transfected with control or *CHROME*-targeting GapmeRs. **h,** Western blot analysis of ABCA1 and HSP90 (control) in hepatocytes transfected with control or *CHROME*-targeting GapmeRs. Molecular weight marker is shown at right. **i,** qPCR analysis of mature and nascent *ABCA1* mRNA transcripts in primary human hepatocytes transfected with control or *CHROME*-targeting GapmeRs. **b, d-i,** Data are the mean ± SEM of 3–5 independent experiments. P-values were calculated using a two-tailed student's t-test. *P≤0.05, **P≤0.01.

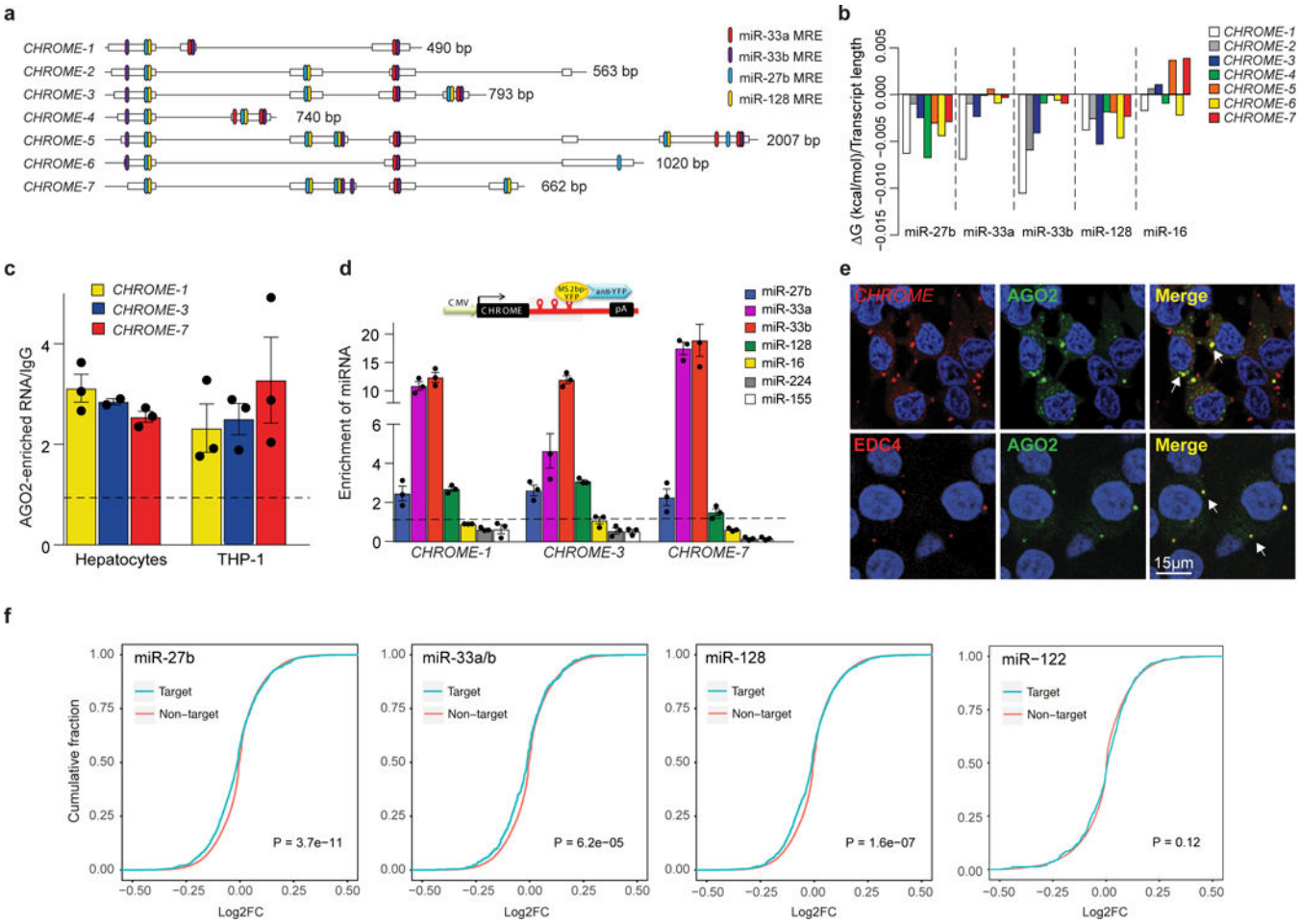

Figure 4. *CHROME* interacts with a set of miRNAs known to repress cholesterol efflux.

a,Schematic diagram showing multiple miRNA response elements (MRE) for miR-27b, miR-33a, miR-33b and miR-128 in CHROME variants. **b,** RNAcofold-predicted changes in Gibbs free energy (ΔG) upon binding of *CHROME* variants to miR-27b, miR-33a, miR-33b, miR-128 or miR-16 (control). **c,** Enrichment of *CHROME* RNA in AGO2-immunoprecipitates from primary human hepatocytes and THP-1 macrophages relative to IgG control. **d,** qPCR detection of miRNAs in *CHROME-1*, *CHROME-3* and *CHROME-7* ribonucleoprotein complexes precipitated using MS2-tagged RNA affinity purification (MS2-TRAP). Data are normalized to *U6* and control MS2-bs-vector. **c-d)** Data are the mean ± SEM of a single experiment and are representative of 3 independent experiments. **e,** Fluorescence *in situ* hybridization for *CHROME* (red: top) and immunostaining for the P-body marker EDC4 (red: bottom) in HEK293T cells expressing AGO2-GFP (green) and stained with DAPI nuclear stain (blue). Arrows in merged image indicate signal colocalization (yellow) in punctate structures. Staining is representative of 2 independent experiments. **f,** Cumulative distribution plots of log2-transformed gene expression fold changes from RNA-Seq of *CHROME*-shRNA vs control-shRNA HepG2 cells (3 biological replicates each), showing genes containing miR-27b, miR-33a/miR-33b or miR-128 target sites predicted by Targetscan (blue) and all other expressed genes (red). As a control, similar analyses were performed for genes containing target sites of miR-122, a hepatic miRNA

with known roles in lipid metabolism. The increased prevalence of negative log2-fold changes among predicted targets of miR-27b, miR-33 and miR-128 (left shift of blue line compared to red), but not miR-122, suggests increased inhibitory effects of those miRNAs upon *CHROME* knockdown. P-values were calculated a two-sample Kolmogorov-Smirnov test.

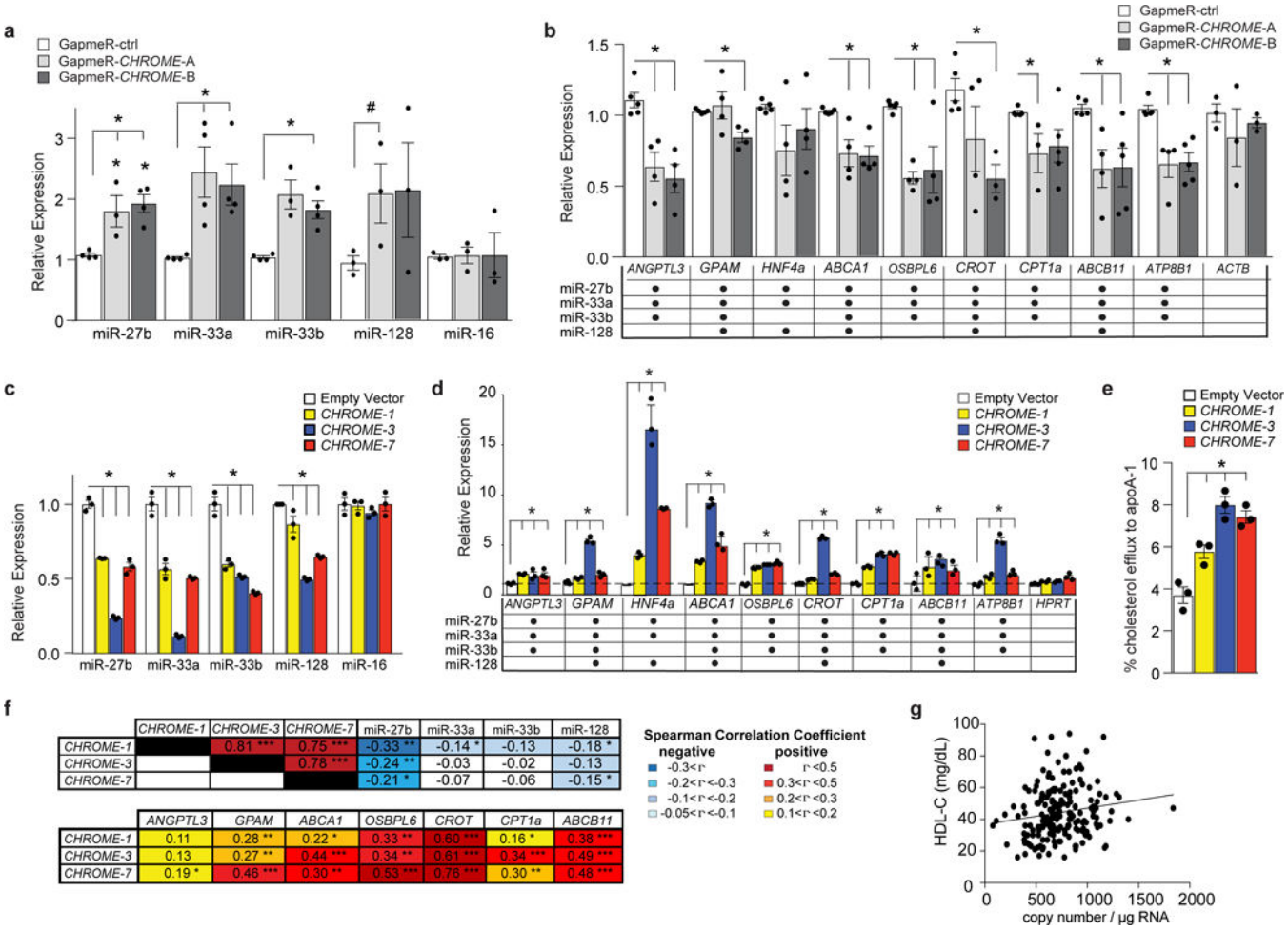

Figure 5. Gain or loss of *CHROME* in hepatocytes alters levels of its interacting miRNAs and their common target mRNAs involved in cholesterol metabolism.

a-d, qPCR analysis of levels of (a, c) miRNAs and (b, d) their common target mRNAs in (a-b) primary human hepatocytes transfected with control (GapmeR-ctrl) or *CHROME*-targeting GapmeRs (GapmeR-*CHROME*-A or GapmeR-*CHROME*-B) or (c-d) HepG2 cells stably expressing *CHROME-1, CHROME-3, CHROME-7* or empty vector. Table in (b) and (d) indicates validated targets of miR-27b, miR-33a, miR-33b and miR-128. **e,** Measurement of cholesterol efflux to exogenous apoA-1 in THP-1 macrophages stably expressing empty vector, *CHROME-1, CHROME-3* or *CHROME-7.* **f,** Spearman rank correlation coefficients (rho) of *CHROME* RNA copy number with its interacting miRNAs and their target mRNAs in human liver (n=200). **g,** Scatter plot showing relationship between hepatic *CHROME-7* copy number and plasma levels of HDL cholesterol (n=200). Spearman correlation coefficients between *CHROME-7* copy number and plasma levels of HDL cholesterol (n=200, rho=0.1722, P=0.0019) were calculated using the SAS statistic software. Data in (a-e) are the mean ± SEM of 3 independent experiments and P-values were calculated using a two-tailed student's t-test. #P≤0.1, *P≤0.05, **P≤0.001, ***P≤0.000001.

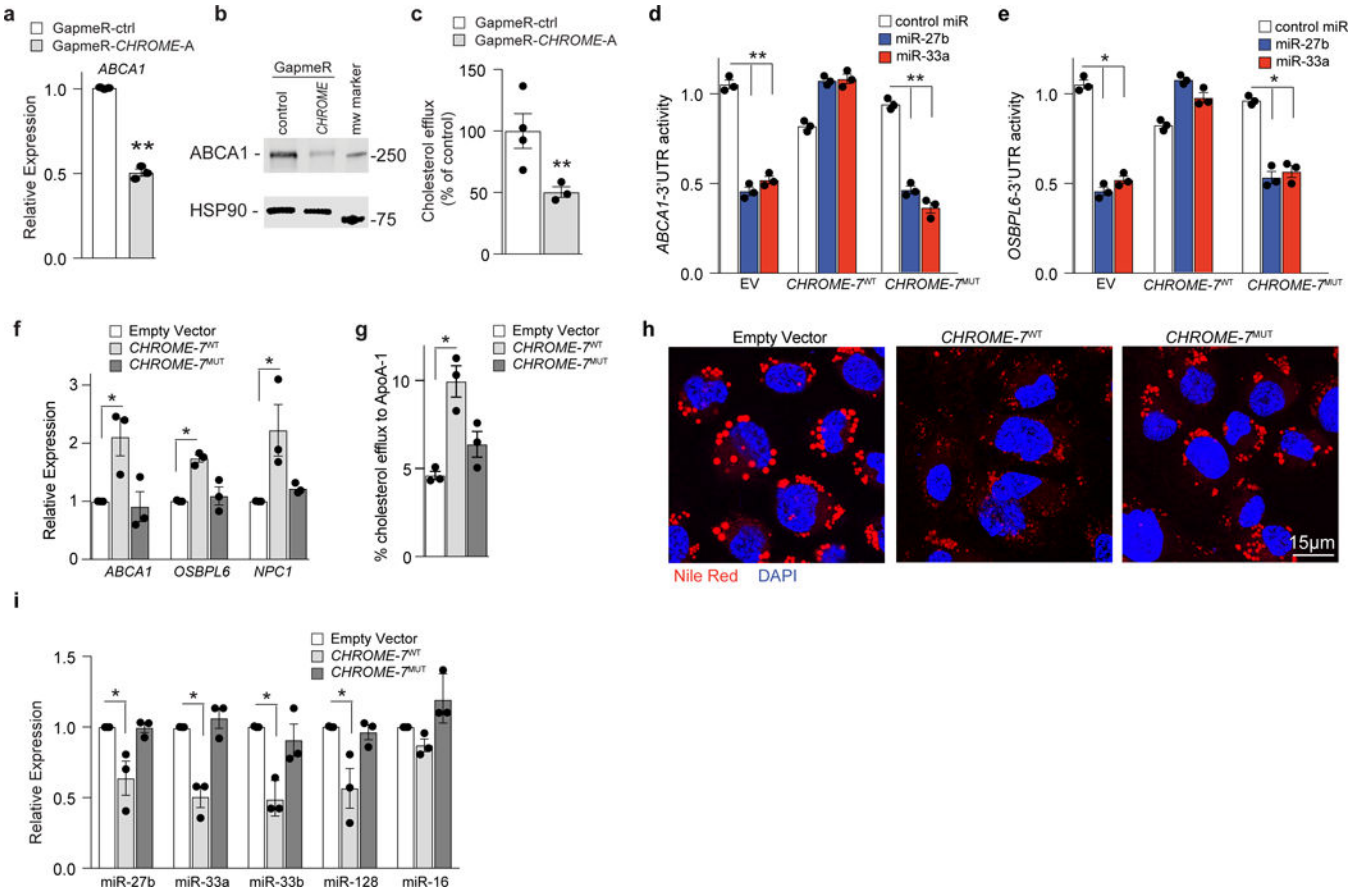

Figure 6. *CHROME* regulates cholesterol efflux in macrophages via its interaction with miRNAs.

a) qPCR analysis of *ABCA1* mRNA in THP-1 macrophages transfected with control (ctrl) or *CHROME*-targeting GapmeRs. Data are the mean ± SEM of 3 independent experiments. (b) Western blot of ABCA1 and HSP90 (internal control) protein in THP-1 macrophages transfected with control (ctrl) or *CHROME*-targeting GapmeRs. Molecular weight marker is shown at right. Data are representative of 3 independent experiments. **c,** Measurement of cholesterol efflux to exogenous apoA-1 in THP-1 macrophages transfected control (ctrl) or *CHROME*-targeting GapmeRs. Data are the mean ± SEM of 4 independent experiments. **d-e**, Activity of (d) *ABCA1*-3'UTR and (e) *OSBPL6*-3'UTR luciferase reporter genes in HEK293T cells expressing empty vector (EV), wild type *CHROME*-7 (*CHROME-7*^{WT}), or *CHROME*-7 with its miR-33, miR-27b and miR-128 binding sites mutated (*CHROME-7*^{MUT}) following treatment with control miR, miR-27b or miR-33 mimics. Data are the mean ± SEM of 3 biological replicates from a single experiment. Data are representative of 3 independent experiments. **f,** qPCR analysis of miR-27b, miR-33 and miR-128 target genes regulating cholesterol efflux in THP-1 macrophages stably expressing empty vector, *CHROME-7*^{WT} or *CHROME-7*^{MUT}. Data are the mean ± SEM of 3 experiments. **g,** Measurement of cholesterol efflux to apoA-1 in THP-1 macrophages stably expressing empty vector, *CHROME-7*^{WT} or *CHROME-7*^{MUT}. Data are the mean ± SEM of 3 experiments. **h,** Representative images of Nile Red stained lipid droplet accumulation in acetylated LDL treated THP-1 macrophages stably expressing empty vector, *CHROME-7*^{WT} or *CHROME-7*^{MUT}. Cells were stained with DAPI (blue) to visualize nuclear DNA. **i,** qPCR

analysis of miRNA levels in THP-1 cells stably expressing empty vector, *CHROME-7*^{WT} or *CHROME-7*^{MUT}. miR-16 is included as a negative control. Data are the mean ± SEM of 3 experiments. P-values were calculated using a two-tailed student's t-test. *P≤0.05, **P≤0.01, ***P≤0.001.